



## Magnification of hydrodynamic coefficients on a flexible pipe fitted with helical strakes in oscillatory flows

Haojie Ren<sup>a,b</sup>, Mengmeng Zhang<sup>a,b,\*</sup>, Jingyun Cheng<sup>c</sup>, Peimin Cao<sup>c</sup>, Yuwang Xu<sup>a,b</sup>, Shixiao Fu<sup>a,b</sup>, Chang Liu<sup>d</sup>, Yifan Wang<sup>a</sup>

<sup>a</sup> State Key Laboratory of Ocean Engineering, Shanghai Jiao Tong University, Shanghai, China

<sup>b</sup> Collaborative Innovation Center for Advanced Ship and Deep-Sea Exploration, Shanghai, China

<sup>c</sup> SBM Offshore, Houston, TX, USA

<sup>d</sup> Department of Mechanical Engineering, Johns Hopkins University, Baltimore, MD, 21218, USA

### ARTICLE INFO

#### Keywords:

Vortex-induced vibration  
Hydrodynamic coefficient  
Helical strakes  
Flexible pipe  
Oscillatory flow

### ABSTRACT

The features of hydrodynamic coefficients including drag and added mass coefficients on a flexible pipe fitted with helical strakes in an oscillatory flow are studied experimentally. The experiment of a flexible straked pipe was conducted in an oscillatory flow with the Keulegan-Carpenter (KC) number varying from 9 to 165 and the maximum reduced velocities ranging from 4 to 8. Strain response in both in-line and cross-flow directions are measured by fiber bragg grating sensors. Using displacement reconstruction and inverse analysis methods, displacement response and hydrodynamic force of the straked pipe are identified. Then, through the least squares method, corresponding drag and added mass coefficients are extracted. The asymmetric features at the acceleration and deceleration stages of hydrodynamic force on a flexible pipe in the in-line direction under oscillatory flow are first observed. Compared with a bare pipe, helical strakes can effectively reduce the higher frequency fluctuating force and enhance the wake effects. The hydrodynamic coefficients on the straked pipe are significantly magnified in the case of a relatively small KC number. The maximum mean drag coefficients can reach approximately 10. The presented work suggests that the risk of helical strakes application should be fully evaluated through flexible pipe experiments in both steady flow and unsteady flow.

### 1. Introduction

As natural gas and oil production extends to deep and ultra-deep-water areas, risers are becoming increasingly slender. Under the ocean currents, vortices are periodically generated and alternately shed from the sides of these very slender risers, resulting in a corresponding periodic excitation force. When the frequency of this force is near one of natural frequencies of a flexible riser, a significant vibration will occur. This is termed as Vortex-induced Vibration (VIV) (Blevins and Saunders, 1977). This periodic vibration has been proven to be the main reason for the fatigue damage of risers. Therefore, researchers in both industry and academia have done many works to find effective ways to suppress VIV.

At present, there are two main methods to suppress VIV of the riser: active and passive control. The main difference between them is that active control requires external power (He et al., 2000; Jeon et al., 2004; Williams and Zhao, 1989), while passive control does not. The latter is more widely used and has been previously studied by many researchers

due to its easier manufacture (Allen et al., 2006; Bearman et al., 1985; Galvao et al., 2008; Gao et al., 2015, 2016; Trim et al., 2005; Vandiver et al., 2006). Among the various forms of passive control, helical strakes are the most widely used apparatuses in practical projects. Although helical strakes serve as an effective VIV suppression device by altering the separation characteristics over the cross section and spanwise direction of the riser, they can also cause a significant magnification in drag and added mass force (API, 1998). These two force components can induce relatively larger deformations and stresses, which affect the structural strength and fatigue life of the riser (Sumer and Fredsøe, 1988). Thus, it is catching more and more attention in engineering applications whether helical strakes will cause some adverse effect on the riser. It is necessary to investigate the magnified effects of drag and added mass coefficients on straked riser when evaluating the VIV suppression efficiency of helical strakes.

To investigate this amplification of drag force in In-Line (IL) direction, Korkischko et al. (2007) presented mean drag coefficients of rigid

\* Corresponding author. State Key Laboratory of Ocean Engineering, Shanghai Jiao Tong University, Shanghai, China.  
E-mail address: [claire\\_zhang@sjtu.edu.cn](mailto:claire_zhang@sjtu.edu.cn) (M. Zhang).

cylinders with different helical stakes, and an expected magnification is observed through towing experiments. The drawback is that this test of stationary rigid cylinder has not considered the influences of VIV response on drag. Quen et al. (2014) presents experiments of flexible straked pipes with pitches equal to 5 D, 10 D, and 15 D and heights equal to 0.05 D, 0.10 D, and 0.15 D under uniform flow. Unexpectedly, based on drag force measured at both ends, a phenomenon that bare cylinders possess higher drag coefficients than the straked pipes is found, which is contrary to beliefs reported by API (1998) (API, 1998). Ren et al. (2019b) first identified drag force and coefficients at each section of a flexible straked pipe with different pitches and heights in uniform flow through the inverse analysis method. The mean drag coefficients of straked pipe are found to be closely related to the geometry of stakes and not necessarily larger than the bare pipe. Drag amplification of bare pipe caused by VIV response through broadening incoming flow area can be as large as helical stakes induced by increasing hydrodynamic diameter and altering the wake. These studies indicate that the application of helical stakes may not adversely affect the riser.

In a real sea state, riser inevitably encounters the action of wave and vessel motions. This wave and wave-induced periodic motion of a platform always result in a relatively equivalent oscillatory flow around risers. Recent experimental study found that the oscillatory flow induced by the vessel motion can also excite the VIV at the sag-bend of steel catenary riser (Wang et al., 2015, 2017), so-called Vessel Motion-induced VIV (VMI-VIV) (Pesce et al., 2017). VMI-VIV can cause serious fatigue damage to risers (Wang et al., 2014). To suppress VMI-VIV, Cheng et al. (2016) and Constantinides et al. (2016) presented a similar experiments of a steel lazy wave riser fitted with helical stakes with a pitch of 15 D and a height of 0.25 D, where D is the diameter of the bare riser. However, VIV still occur for the straked pipe and its suppression efficiency is not as good as that in the steady flow. Aiming at this phenomenon, Ren et al. (2019a) conducted a straked pipe with the same pitch of 15 D and height of 0.25 D in an equivalent oscillatory flow by forcing the model to oscillate in still water with different periods and amplitudes. A surprising result is that the suppression efficiency can be reduced to 50% in an oscillatory flow under small Keulegan-Carpenter (KC) number. The characteristics of helical stake in the oscillatory flow attracted the attention. The combination of more obvious VIV phenomenon and helical stakes may lead to more pronounced amplified effects on hydrodynamic coefficients. This will bring more concerns about these adverse effects of helical stakes in application. Thus, further research is required to reveal the hydrodynamic coefficients features of the straked flexible pipes undergoing VIV in an oscillatory flow.

In this paper, the remainder is organized as follows. Section 2 presents the VIV model tests for a straked pipe in an equivalent oscillatory flow. It should be noted that the straked pipe model has the same pitch of 15 D and height of 0.25 D as Ren et al. (2019a). The KC numbers varied between 9 and 165, and the maximum reduced velocities ranged from 4 to 8. In Section 3, the identification methods of hydrodynamic force and coefficients on helical stakes in the IL direction are firstly proposed. The features of hydrodynamic force and coefficients under different maximum reduced velocities and KC numbers are presented in Section 4. Finally, investigated conclusions based on the observation are summarized in Section 5.

#### Nomenclature

$L$	Length of test model (m)	$\rho$	Density of the water, $\rho = 1000 \text{ kg/m}^3$
$D$	Outer diameter of the tested bare pipe (m)	$m$	Mass of straked pipe per unit length in still water ( $\text{kg/m}$ )
$\bar{m}_s$	Mass of straked pipe per unit length in air ( $\text{kg/m}$ )	$\text{Re}_{\max}$	Maximum Reynolds number
$\bar{m}_b$	Mass of bare pipe per unit length in air ( $\text{kg/m}$ )	$\nu$	Kinematic viscosity coefficient ( $\text{m}^2 \text{ s}^{-1}$ )
$EI$	Bending stiffness ( $\text{N}\cdot\text{m}^2$ )	$\varepsilon_{IL}(z,t)$	Bending strain in the IL direction
$EA$	Tensile stiffness (N)		

(continued on next column)

(continued)

Nomenclature		
	$\varepsilon_{IL,b}(z,t)$	Original strain sampled by IL_b measurement points
$F_{T0}$	Pre-tension (N)	$\varepsilon_{IL,d}(z,t)$ Original strain sampled by IL_d measurement points
$\zeta_b$	Damping ratio of the bare pipe	$\varepsilon_{CF}(z,t)$ Bending strain in the CF direction
$x(t)$	Displacement of forced motion (m)	$f_0$ Forced oscillation frequency (Hz)
$U(t)$	Velocity of forced motion (m/s)	$x(z,t)$ Displacement response in the IL direction (m)
$A_m$	Forced oscillation amplitude (m)	$p_i(t)$ The $i$ th generalized coordinate displacement values
$T$	Forced oscillation period (s)	$\phi_i(z)$ Displacement of the $i$ th modal shape
$t$	Time (s)	$\kappa(z,t)$ Curvature in the IL direction
$V_R$	Maximum reduced velocity	$\phi_i''$ The $i$ th modal shape of the curvature
$f_{10}$	The 1st natural frequency of straked pipe in still water (Hz)	$F(z,t)$ Hydrodynamic force per unit length in the IL direction (N/m)
$F_T(t)$	Tension force (N)	$C$ Damping coefficient
$F^*(z,t)$	Predicted hydrodynamic force (N)	$C_D(z)$ Drag coefficient
$C_m(z)$	Added mass coefficient	$J$ Squared difference between the predicted and identified force (N/m)
$n$	Sample number	$f_{st}$ Vortex shedding frequency (Hz)
$St$	Strouhal number	$f_1$ The 1st eigen frequency under time-varying tension (Hz)
$f_2$	The 2nd eigen-frequency under time-varying tension (Hz)	$\eta$ Suppression efficiency (%)
$Y_{\max}$	Maximum standard deviation of the displacement for bare pipe (m)	$Y_{s,\max}$ Maximum standard deviation of the displacement for straked pipe (m)
$ U /$	$(f_1^* D)$	Instantaneous reduced velocity
$\bar{C}_D$	Mean drag coefficient	
$\bar{C}_m$	Mean added mass coefficient	$R$ Radius of the flexible pipe model (m)
$Y_d$	The maximum deformation caused by the gravity of the flexible pipe (m)	$F_{\max}$ The maximum range of force transducer (N)
$F_{T0}$	Pretension force (N)	$h$ Height of helical stake (m)
$p$	Pitch of helical stake (m)	$\zeta_s$ Damping ratio of the straked pipe
$U_m$	The forced motion velocity amplitude (m/s)	$f_{b-10}$ Calculated first natural frequency of bare pipe in still water (Hz)
$X_{RMS}(z)$	The RMS value of displacement response at the position $z$ in the IL direction (m)	$Y_{RMS}(z)$ The RMS value of displacement response at the position $z$ in the CF direction (m)
$X(z,t_i)$	The displacement response at the position $z$ and time $t_i$ in the IL direction (m)	$Y(z,t_i)$ The displacement response at the position $z$ and time $t_i$ in the CF direction (m)
$\varepsilon_{IL-RMS}$	The RMS value of strain response in the IL direction	$\varepsilon_{CF-RMS}$ The RMS value of strain response in the CF direction
$Y_{RMS-B}(z)$	The RMS value of displacement response of the bare pipe at the position $z$ in the CF direction (m)	$Y_{RMS-S}(z)$ The RMS value of displacement response of the straked pipe at the position $z$ in the CF direction (m)

## 2. Model test

### 2.1. Test apparatus

A model test was performed in an ocean basin at Shanghai Jiao Tong University. The entire test apparatus containing primarily two horizontal and vertical linear motion tracks and a flexible pipe model were

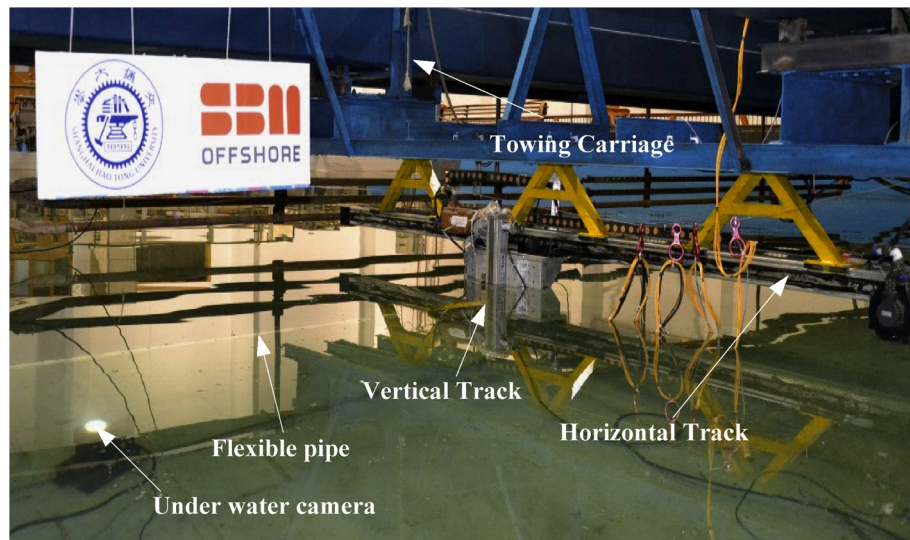


Fig. 1. Overview of the whole experimental setup.

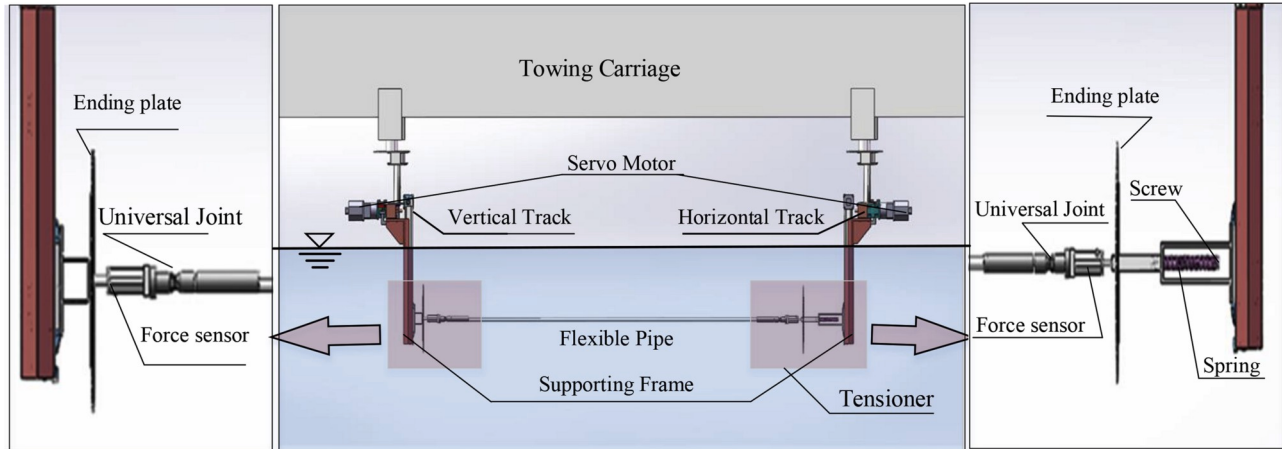


Fig. 2. Detail sketches of all devices used during experiments.

**Table 1**  
Parameters of the flexible pipe model.

Item	Value
Model length L (m)	4
Outer diameter D (mm)	29
Mass of straked pipe in air $\bar{m}_s$ (kg/m)	1.696
Mass of bare pipe in air $\bar{m}_b$ (kg/m)	1.529
Bending stiffness EI ( $N \cdot m^2$ )	46.433
Tensile stiffness EA (N)	1.528E+06
Pre-tension $F_{T0}$ (N)	500
Damping ratio $\zeta_b$ of bare pipe	2.53%
Damping ratio $\zeta_s$ of straked pipe	2.66%
Calculated first natural frequency of straked pipe $f_{10}$ in still water (Hz)	1.8
Calculated first natural frequency of bare pipe $f_{b-10}$ in still water (Hz)	1.9

mounted under the bottom of a measuring bridge of ocean basin as shown in Fig. 1 and Fig. 2. Two force sensors are placed at two ends of the pipe model through universal joints. A tensioner connected to the force sensor was fixed to the slider of the vertical track. Two endplates were used to reduce the disturbance of the supporting frame to the equivalent oscillatory flow field.

In our experiments, a pretension force of 500N was selected and applied to the flexible pipe through tensioner, which consists of a lead

screw and a spring. When the screw is tightened, the spring is compressed and applies the force on screw, which is connected with force sensor and the flexible pipe as shown in Fig. 2. Thus, the pretension force along the axis of flexible pipe was loaded.

For the pretension force, the two justifications should be considered: (1) avoiding significant deformation caused by the gravity of the flexible pipe; (2) ensuring that the expected motion under the different maximum reduced velocity and KC numbers can be achieved within the allowable range of experimental apparatus.

To check these two points, the finite element model was built according to the parameters list in Table 1 through ANSYS software. The maximum deformation  $y_d$  at the middle point of flexible pipe in the still water was calculated and about 0.038m and we think this small deformation can be allowed. Beyond that, the maximum range of force transducer  $F_{max}$  is 1000N and the VIV and drag force will cause the amplification of tension force. To ensure that the force sensor has a certain safety, the pretension force  $F_{T0}$  of 500N is finally selected. All the aspects meet the above two requirements.

The flexible pipe was made up of a polypropylene random pipe that is filled with copper cable inside. Silicone gel was placed between different layers to prevent relative slippage. The helical strakes were tied to the flexible pipe. The main properties of the test model are listed in Table 1. The geometric sketch of helical strakes in this experimental

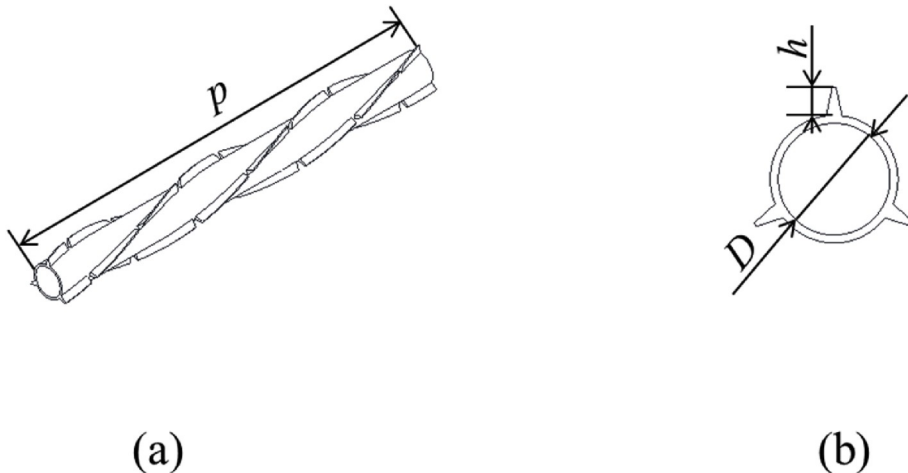


**Fig. 3.** Geometric parameters of the helical strakes: (a) axonometric drawing; (b) cross section sketch.

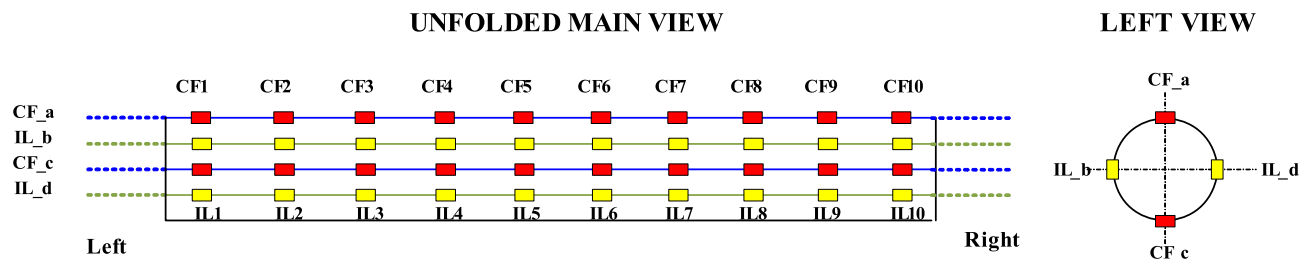


**Fig. 4.** FBG strain sensor instrumentation along the flexible pipe model.

study is shown in Fig. 3. The height  $h$  and pitch  $p$  are respectively 0.25 D, 15 D. The start number of this helical stike is 3. Four groups of Fiber Bragg Grating (FBG) strain sensors were installed to measure the strain responses in both the Cross-Flow (CF) and IL directions. Each of the FBG groups (CF\_a, CF\_c, IL\_b and IL\_d) had ten measurement points along the pipe separated by 0.36 m, as shown in the schematic diagram in Fig. 4.

## 2.2. Test matrix

To investigate drag and added mass coefficients on the flexible pipe fitted with helical strakes in an oscillatory flow, the model was forced to oscillate in harmonic motions under various combinations of amplitude and period in the horizontal direction. The instantaneous displacement  $X(t)$  and velocity of the forced motion  $U(t)$  can be expressed as follows:

$$X(t) = A_m \sin\left(\frac{2\pi}{T} t\right) \quad (1)$$

$$U(t) = A_m \frac{2\pi}{T} \cos\left(\frac{2\pi}{T} t\right) \quad (2)$$

where  $A_m$  and  $T$  are oscillation amplitude and period, respectively.

The drag and added mass coefficient are related to the VIV response. The KC number and the maximum reduced velocity  $V_R$  are considered as two main parameters that determine the VIV characteristics of a flexible cylinder under oscillatory flow (Fu et al., 2014; Sumer and Fredsøe, 1988), as well as the hydrodynamic coefficient. The KC number and  $V_R$  can be presented as Eq. (3) and Eq. (4), respectively.

$$KC = \frac{2\pi \cdot A_m}{D} \quad (3)$$

$$V_R = \frac{2\pi \cdot A_m}{T f_{10} \cdot D} \quad (4)$$

**Table 2**  
Test matrix.

Case No.	$V_R$	$A_m$ (m)	KC	$Re_{max}$
1–19	4	[0.04:0.02:0.76]	9–165	5240
20–40	6	[0.04:0.02:0.76]	9–165	7860
41–61	8	[0.04:0.02:0.76]	9–165	10,455

where  $f_{10}$  denotes the first natural frequency of the test model in still water.  $f_{10} = 1.8$  Hz is used here considering that the first natural mode is the potential excitation mode for all the test cases, which can be calculated by Eq. (5):

$$f_{n0} = \frac{n}{2L} \sqrt{\frac{F_{T_0}}{m} + \frac{n^2 \pi^2 EI}{L^2 m}}, m = \bar{m}_s + \frac{1}{4}\pi D^2 \rho C_m \quad (C_m = 1.0), n = 1, 2, \dots \quad (5)$$

where  $F_{T_0}$  is the pretension force.  $m_s$  is the mass of straked pipe per unit length in still water.  $L$  and  $D$  are the length and diameter of flexible pipe, respectively.  $EI$  is the bending stiffness of pipe.  $\rho$  is the density of water,  $\rho = 1000 \text{ kg/m}^3$ . The added mass coefficient is chosen as  $C_m = 1.0$ . Notably, the added mass may deviate from the value of 1.0 in still water, and the forced oscillation periods will change with the KC number at the same maximum reduced velocity. In addition, it should be noted that the diameter values are all kept the same as that of bare pipe.

All of test cases were divided into four groups with different maximum reduced velocities, as presented in Table 2. The corresponding maximum Reynolds number ( $Re_{max}$ ) has also been listed in this table, which can be calculated by Eq. (6):

$$Re_{max} = \frac{U_m D}{\nu} \quad (6)$$

where  $U_m$  is the forced motion velocity amplitude.  $\nu$  is the kinematic

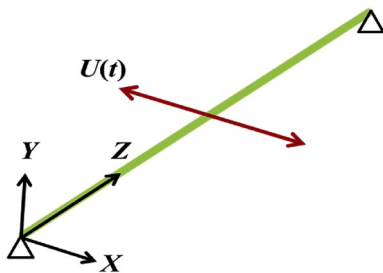


**Fig. 5.** Definition of coordinate system on a flexible pipe under an oscillatory flow.

viscosity coefficient. In our experiment, the ambient temperature is maintained near 15 °C and  $\nu$  is therefore approximately  $1.14 \times 10^{-6} \text{ m}^2 \text{ s}^{-1}$ . The maximum reduced velocity varied from 4 to 8.  $Re_{\max}$  located in the region of approximately  $5 \times 10^3$  to  $1 \times 10^4$ . Each test group had test cases with a KC number ranging from 9 to 165 under the same amplitude of the forced motion velocity. The same cases were also conducted for a bare pipe. The effects of helical strakes on hydrodynamic coefficients will be easily revealed through above cases with and without helical strakes.

### 3. Basic theory

#### 3.1. Preprocessing

For the convenience of description, the coordinate system is defined as O-XYZ; the origin is at one end point of the pipe and the Z-axis, X-axis and Y-axis are along the axis of the pipe, the IL direction, and the CF direction, respectively, as shown in Fig. 5.

At the start of experiments, a constant pre-tension of 500N was exerted at the flexible pipe ends. However, the pre-tension periodically varied with pipe oscillation. Thus, the measured strain included three components: the initial axial strain caused by pre-tension, the varying axial strain caused by varying tension and the bending strain caused by oscillatory flow. Thus, the bending strain  $\epsilon_{IL}(z,t)$  caused by the hydrodynamic force in the IL direction can be calculated by Eq. (7):

$$\epsilon_{IL}(z,t) = [\epsilon_{IL\_b}(z,t) - \epsilon_{IL\_d}(z,t)] / 2 \quad (7)$$

where  $\epsilon_{IL\_b}(z,t)$  and  $\epsilon_{IL\_d}(z,t)$  are the original strain time histories at the z location sampled by IL\_b and IL\_d measurement points, respectively. The pure VIV strain at the z location  $\epsilon_{CF}(z,t)$  can be also calculated using the same methods.

Then, a band-pass filter was utilized to eliminate the higher frequency noise in the IL direction and to remove corresponding higher frequency noise and effects of pendulum motion caused by forced motion in the CF direction. The cutoff frequencies of the band-pass filter were 0 Hz and 15 Hz for the IL direction and  $2.5f_0$  ( $f_0$  is the forced oscillation frequency) and 15 Hz for the CF direction.

#### 3.2. Displacement reconstruction

The displacement reconstruction method is a basic tool for the VIV study (Lie and Kaasen, 2006; Ren et al., 2019a; Song et al., 2017). According to the Euler-Bernoulli beam theory, displacement response of a flexible pipe under the external load can be expressed as the sum of the mode shapes multiplied by the generalized coordinate values in each step. Taking the response in the IL direction as an example, the displacement response  $x(z,t)$  can be expressed as,

$$x(z,t) = \sum_{i=1}^n p_i(t) \phi_i(z), \quad z \in [0, L] \quad (8)$$

where  $p_i(t)$  is the ith generalized coordinate displacement values at time

$t$ ;  $\phi_i(z)$  is the displacement at the position z in the ith modal shape.

Based on small deformation assumption, the curvature  $\kappa(z,t)$  can be expressed as:

$$\kappa(z,t) = \frac{\partial^2 x(z,t)}{\partial z^2} = \sum_{i=1}^n p_i(t) \phi_i''(z), \quad z \in [0, L] \quad (9)$$

where  $\phi_i''$  is the ith modal shape of the curvature. According to the geometric relationship between the curvature and strain, the strain can be calculated by

$$\epsilon_{IL}(z,t) = \kappa(z,t)R = R \sum_{i=1}^n p_i(t) \phi_i''(z), \quad z \in [0, L] \quad (10)$$

where R denotes the radius of the flexible pipe model at the z position.

In this model, modal shapes of the displacement are sinusoidal, which can be expressed as:

$$\phi_i(z) = \sin \frac{i\pi z}{L}, \quad i = 1, 2, \dots \quad (11)$$

From Eq. (9), the modal shapes of the curvature are also sinusoidal. After obtaining the modal shape of the displacement and curvature, the generalized coordinates can be obtained from Eq. (10). Then, the displacement response in the IL direction can be calculated by Eq. (8). Using the same method as previously mentioned, the displacement response of the CF direction can be also obtained.

#### 3.3. Inverse identification of hydrodynamic forces and coefficients

According to the governing equation of a tensioned Euler-Bernoulli beam in the IL direction, the hydrodynamic force can be inversely identified as presented by

$$F(z,t) = \bar{m}_s \frac{\partial^2 x(z,t)}{\partial t^2} + C \frac{\partial x(z,t)}{\partial t} - F_T(t) \frac{\partial^2 x(z,t)}{\partial z^2} + EI \frac{\partial^4 x(z,t)}{\partial z^4} \quad (12)$$

where  $\bar{m}_s$  is mass of straked pipe per unit length in air; C is damping coefficient of the pipe,  $C = 4\pi\zeta\bar{m}_s f_{10}$ ;  $F_T(t)$  is the time-varying axial tension force; EI is the bending stiffness;  $F(z, t)$  is the hydrodynamic force at the z position of t time in the IL direction;  $\partial^2 x(z, t) / \partial t^2$  and  $\partial x(z, t) / \partial t$  represent respectively the acceleration and velocity response in the IL direction, which are calculated using the central difference method of the first and second order partial derivatives with respect to t;  $\partial^2 x(z, t) / \partial z^2$  and  $\partial^4 x(z, t) / \partial z^4$  are respectively the second- and fourth-order spatial derivatives of the displacement in the IL direction, which are also calculated by the central difference method of second and fourth order partial derivatives with respect to z.

According to the Morison equation (Morison et al., 1950, 1953), the total force in the IL direction can be decomposed into two components, i.e., the drag force related to the square of velocity and the inertial force proportional to the acceleration, which can be expressed as,

$$F^*(z,t) = -\frac{1}{2} \rho D C_D(z) \left( U(t) \left| \frac{\partial x(z,t)}{\partial t} \right| - \left( U(t) - \frac{\partial x(z,t)}{\partial t} \right) \right| + C_m(z) \rho \frac{\pi D^2 l}{4} \left[ - \left( \frac{\partial U(t)}{\partial t} - \frac{\partial^2 x(z,t)}{\partial t^2} \right) \right] \quad (13)$$

where  $F^*(z, t)$  represents the predicted force by Morison formula at the z position of the t time;  $C_D(z)$  and  $C_m(z)$  are the drag and added mass coefficients at z position, respectively;  $\rho$  is the density of water,  $\rho = 1000 \text{ kg/m}^3$ .

For convenience in description, it is assumed that

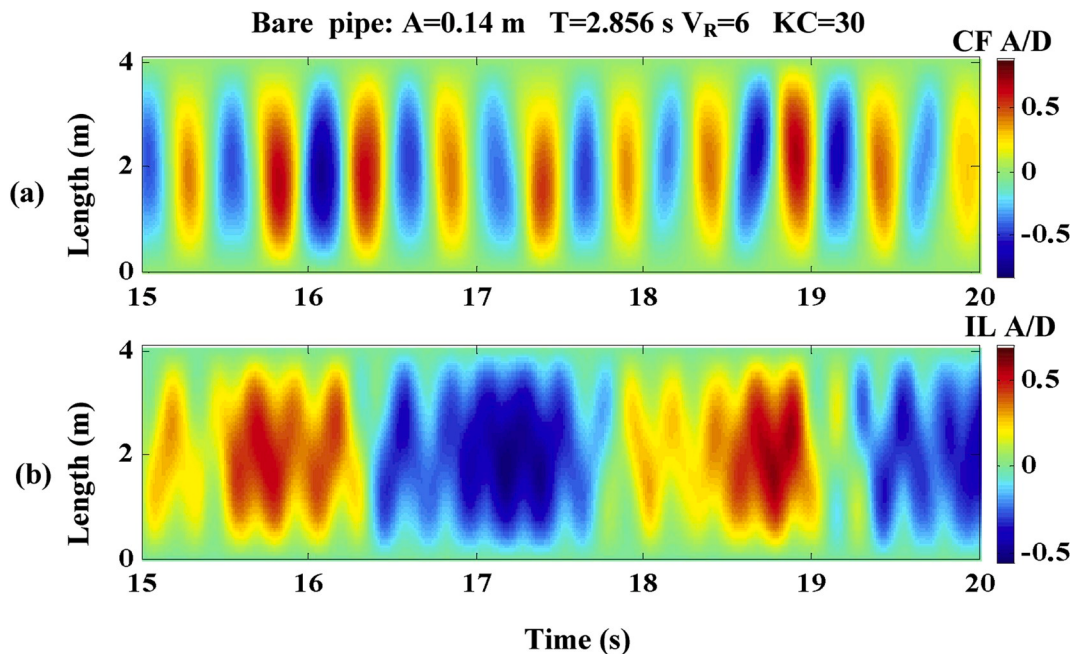


**Fig. 6.** Spatial and temporal distributions of the displacement response of the bare pipe in CF and IL directions in the case of  $V_R = 6$  and  $KC = 30$ . (a) Displacement response in the CF direction; (b) Displacement response in the IL direction.

$$\begin{aligned} C_1(z, t) &= -\frac{1}{2}\rho D \left( U(t) - \frac{\partial x(z, t)}{\partial t} \right) - \left( U(t) - \frac{\partial x(z, t)}{\partial t} \right) \\ C_2(z, t) &= \rho \frac{\pi D^2 l}{4} \left[ -\left( \frac{\partial U(t)}{\partial t} - \frac{\partial^2 x(z, t)}{\partial t^2} \right) \right] \end{aligned} \quad (14)$$

Then, Eq. (13) can be simplified as,

$$F^*(z, t) = C_D(z) \cdot C_1(z, t) + C_m(z) \cdot C_2(z, t) \quad (15)$$

The least squares method is utilized to fit the drag and added mass coefficients in the IL direction.  $C_D(z)$  and  $C_m(z)$  can be obtained by minimizing the sum of the squared difference  $J(C_D(z), C_m(z))$  between

the predicted and identified force, which can be expressed as,

$$\begin{aligned} [\hat{C}_D(z), \hat{C}_m(z)] &= \operatorname{argmin} J(C_D(z), C_m(z)) \\ \text{where } J(C_D(z), C_m(z)) &= \sum_{i=1}^n [F(z, t) - F^*(z, t)]^2 \end{aligned} \quad (16)$$

where  $n$  is the sample number.

To minimize the difference between the identified value and the predicted value of the hydrodynamic force, the following Eq. (17) should be satisfied,

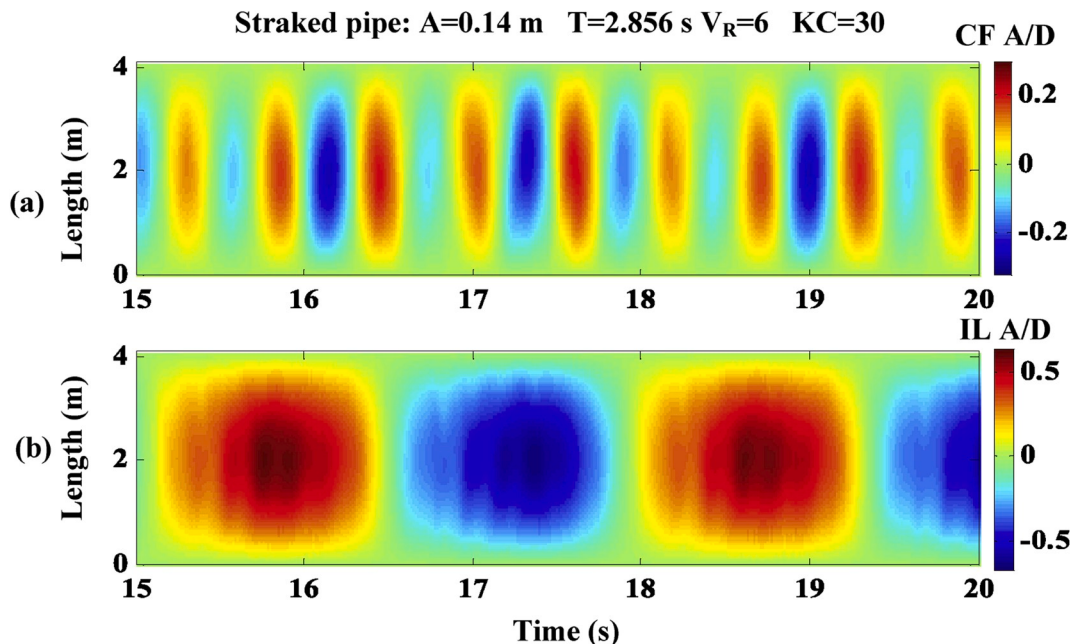


**Fig. 7.** Spatial and temporal distributions of the displacement response of the straked pipe in CF and IL directions in the case of  $V_R = 6$  and  $KC = 30$ . (a) Displacement response in the CF direction; (b) Displacement response in the IL direction.

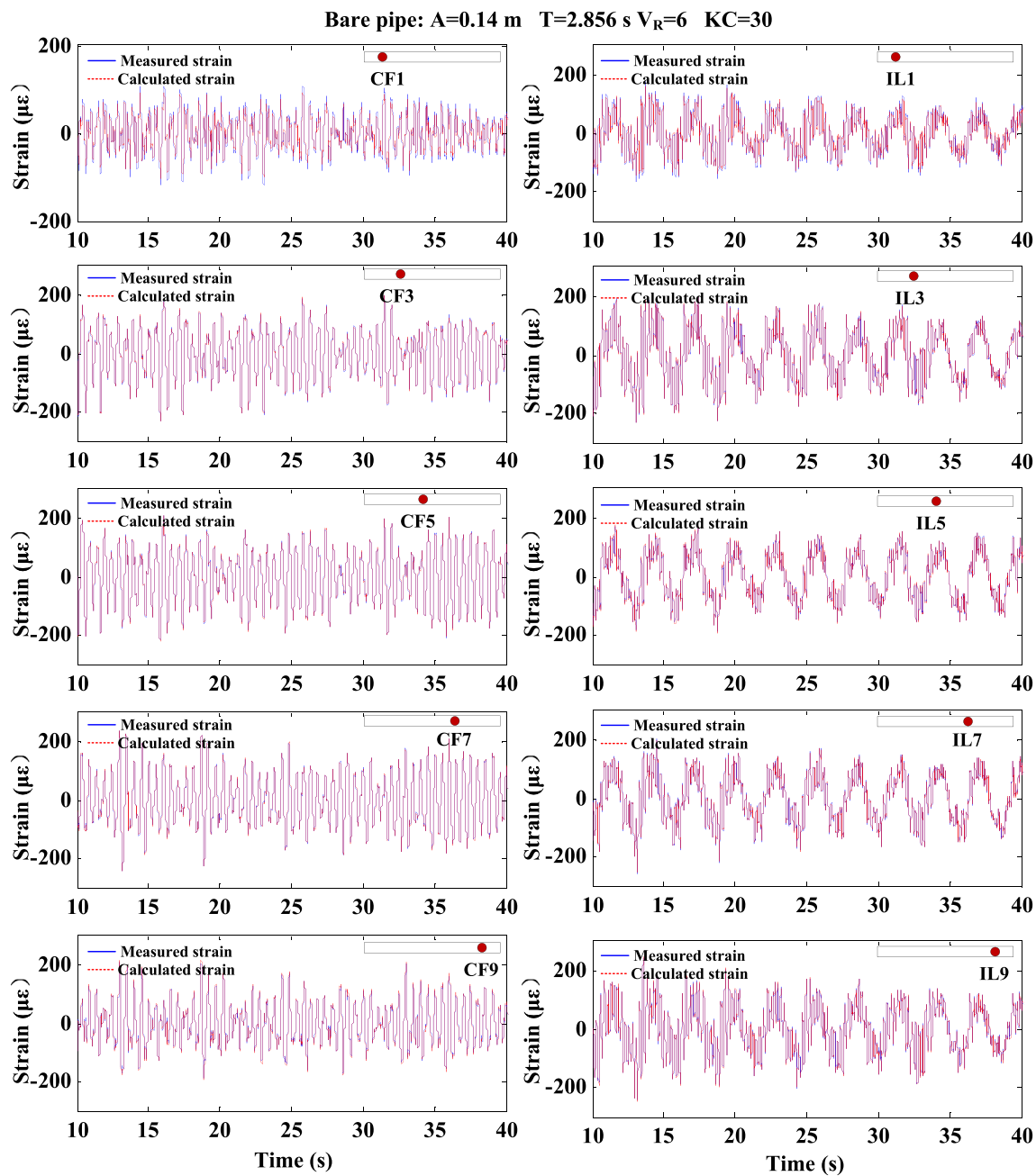


**Fig. 8.** Time history of measured and calculated strain at different gauge points of bare pipe in both CF and IL directions in the case of  $V_R = 6$  for  $KC = 30$ .

$$\frac{\partial J(C_D(z), C_m(z))}{\partial C_D(z)} = 0, \quad \frac{\partial J(C_D(z), C_m(z))}{\partial C_m(z)} = 0 \quad (17)$$

Transforming Eq. (17) into matrix form,

$$\mathbf{H}\mathbf{H}^T \begin{bmatrix} C_D(z) \\ C_m(z) \end{bmatrix} = \mathbf{H}\mathbf{F} \quad (18)$$

where,

$$\mathbf{H} = \begin{bmatrix} C_1(z, t_1) & C_1(z, t_2) & \dots & C_1(z, t_n) \\ C_2(z, t_1) & C_2(z, t_2) & \dots & C_2(z, t_n) \end{bmatrix}, \quad \mathbf{F} = \begin{bmatrix} F(z, t_1) \\ F(z, t_2) \\ \vdots \\ F(z, t_n) \end{bmatrix} \quad (19)$$

Then, the drag and added-mass coefficients can be expressed as:

$$\begin{bmatrix} C_D(z) \\ C_m(z) \end{bmatrix} = (\mathbf{H}\mathbf{H}^T)^{-1} \mathbf{H}\mathbf{F} \quad (20)$$

In this paper, more than 20 oscillation periods are used to reconstruct the hydrodynamic forces and coefficients.

#### 4. Results and discussions

##### 4.1. VIV responses of the flexible pipe

Based on the displacement reconstruction method, the displacement responses of the bare and straked pipe in both CF and IL direction are obtained as shown in Fig. 6 and Fig. 7, respectively. The depth of color represents the magnitude of displacement response. The VIV responses of straked and bare pipe in the CF direction were all observed. More obvious higher frequency components of the displacement responses that is VIV in the IL direction were found in bare pipe. To further investigate the statistical differences in the displacements of bare and straked pipe, the root mean square (RMS) of the displacement responses

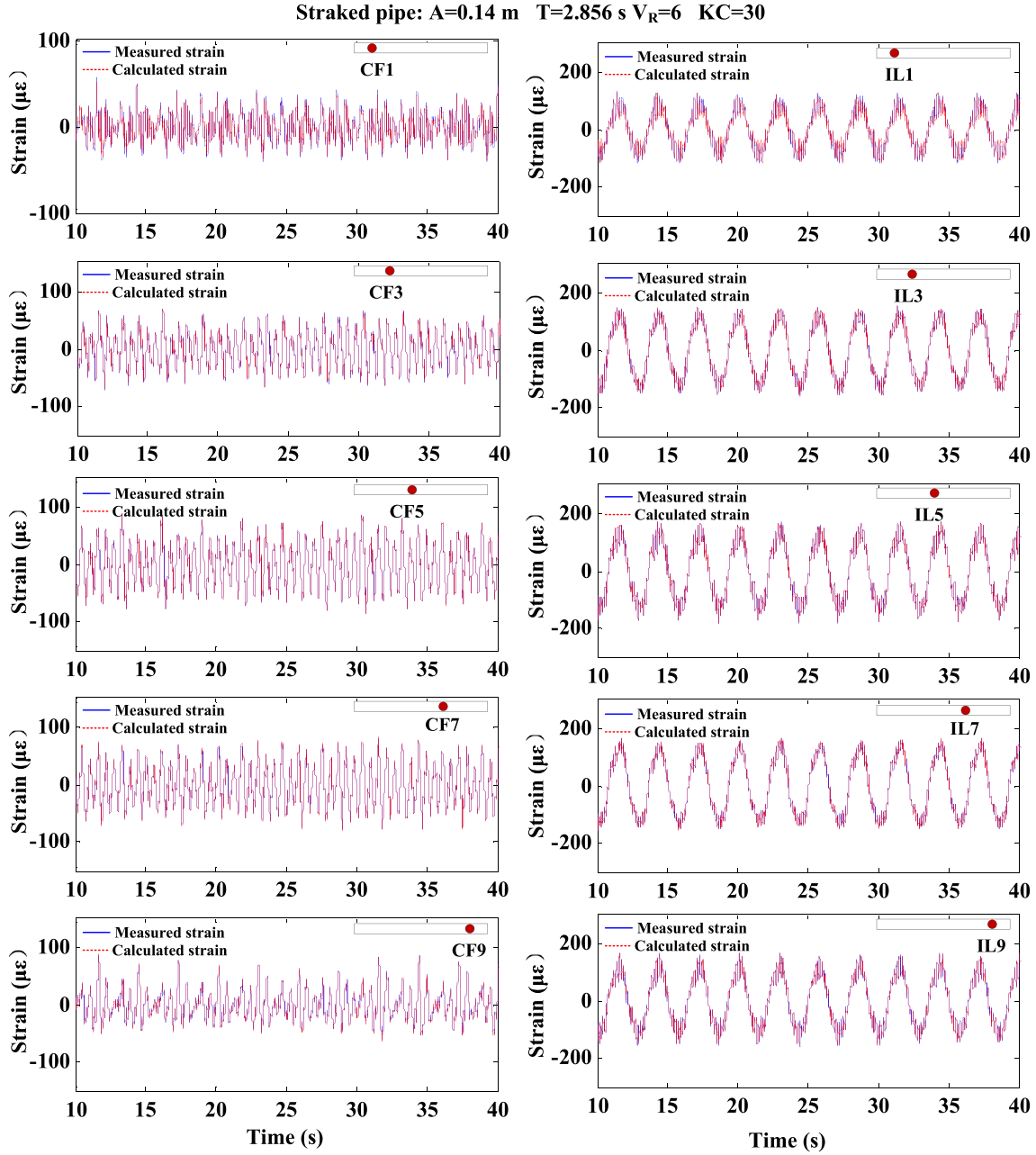


**Fig. 9.** Time history of measured and calculated strain at different gauge points of straked pipe in both CF and IL directions in the case of  $V_R = 6$  for  $KC = 30$ .

were defined as,

$$Y_{RMS}(z) = \sqrt{\frac{1}{n} \sum_{i=1}^n Y^2(z, t_i)} \quad (21)$$

$$X_{RMS}(z) = \sqrt{\frac{1}{n} \sum_{i=1}^n X^2(z, t_i)} \quad (22)$$

where  $Y_{RMS}(z)$  and  $X_{RMS}(z)$  are the RMS value of displacement response at the position  $z$  in CF and IL directions, respectively.  $Y(z, t_i)$  and  $X(z, t_i)$  are the displacement response at the position  $z$  and time  $t_i$  in CF and IL directions, respectively. It should be noted that displacement responses at statistically steady state are used to compute RMS values, which does not include the response time history of initial and ending parts for statistical analysis. Using the same methods, the RMS values of strain response in CF and IL directions ( $\varepsilon_{CF-RMS}$ ,  $\varepsilon_{IL-RMS}$ ) can also be obtained.

**Fig. 10** shows the distribution of RMS values of displacement and strain response along the flexible pipe in the case of  $V_R = 6$  for  $KC = 30$ . As shown in **Fig. 10** (a) and (b), the blue solid line and red dash line represent the displacement response of bare and straked pipe, respectively. The vortex-induced vibration in the CF direction of the straked pipe is obviously smaller than that of the bare pipe, while displacement response in the IL direction of the straked pipe is larger than that of bare one. It indicates that helical strakes can suppress the VIV in CF direction but will magnify the drag force in an oscillatory flow at  $V_R = 6$  and  $KC = 30$ .

To verify the displacement reconstruction method, the bending strain responses of the bare and straked pipe were recalculated through Eq. (10) based on the generalized coordinate displacement value and modal shape of the curvature as shown in **Fig. 8** and **Fig. 9**, respectively. The blue solid and red dash line represent respectively the measured and calculated values. The RMS values of calculated bending strain is compared with the measured one as presented in **Fig. 10** (c) and **10(d)**.

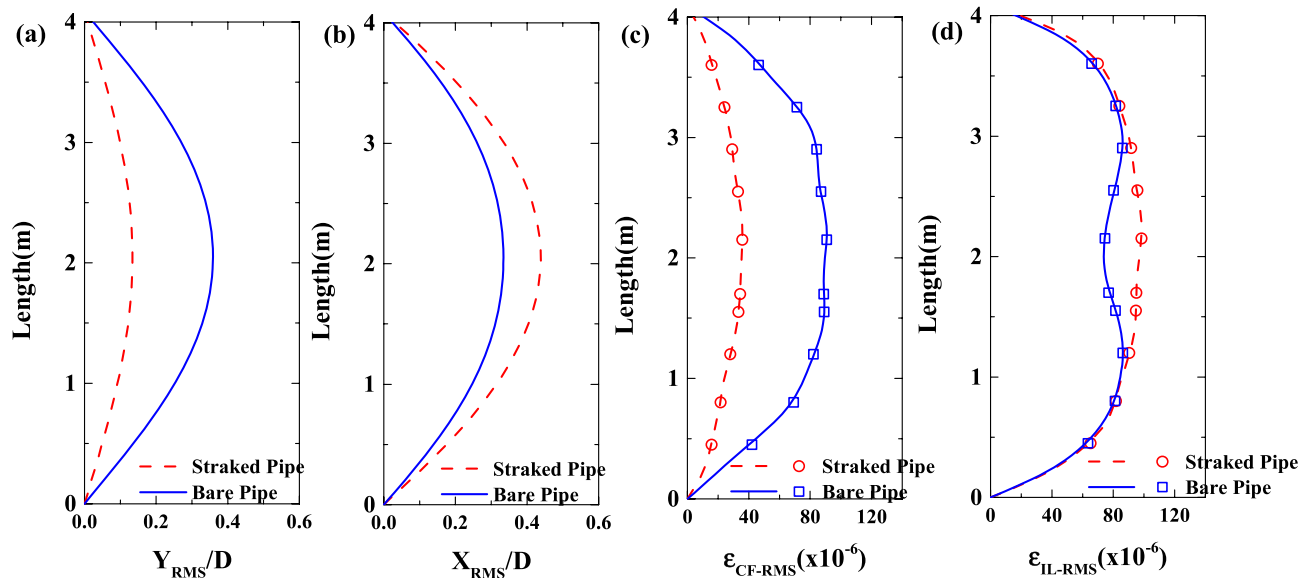


**Fig. 10.** Distribution of displacement and strain response along the flexible pipe in the case of  $V_R = 6$  for  $KC = 30$ : (a) displacement in the CF direction; (b) displacement in the IL direction; (c) strain in the CF direction; (d) strain in the IL direction ( $\square$  measured strain of bare pipe,  $\circ$  measured strain of straked pipe).

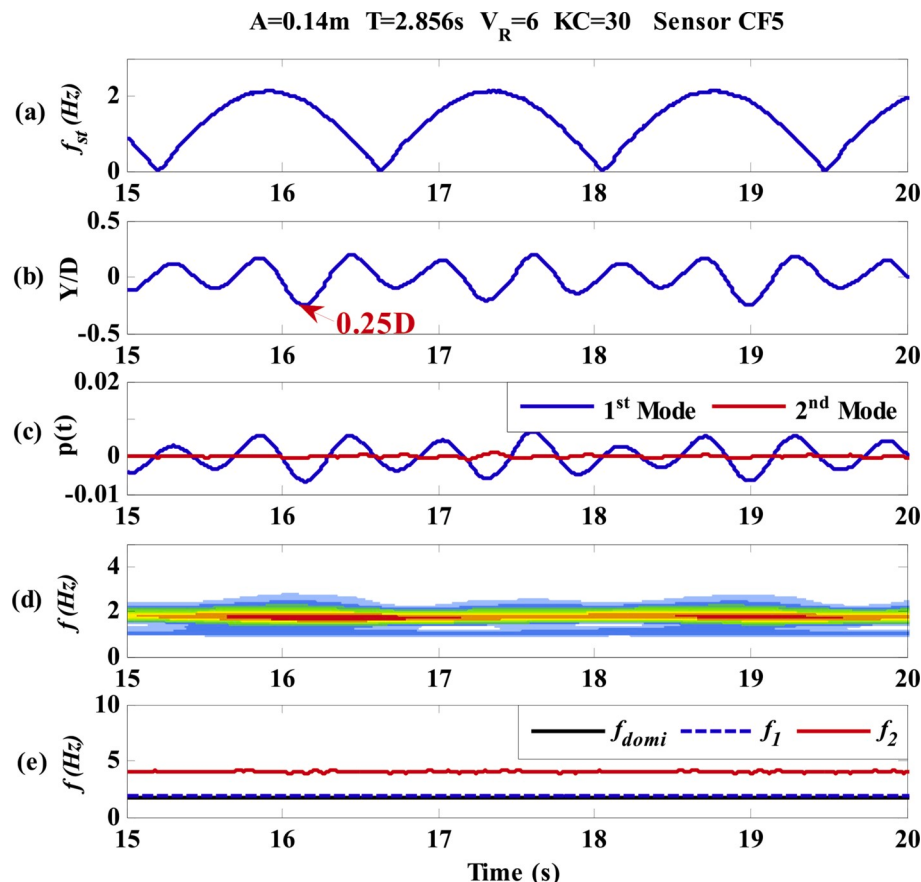


**Fig. 11.** Time history of the VIV response and time-varying frequency distribution in the CF direction at the 5th gauge point of the straked pipe in the case of  $V_R = 6$  and  $KC = 30$  (a) Time-varying frequency of the vortex shedding; (b) VIV displacement response; (c) Modal weight of displacement; (d) Time-varying response frequency obtained by Wavelet analysis; (e) Time-varying natural frequency and dominant response frequency.

Blue solid line and red dash line represent respectively the calculated bending strain of the bare and straked pipe. The blue squares and red circles represent corresponding measured bending strains. From Figs. 8, Fig. 9, Fig. 10 (c) and Fig. 10 (d), the calculated values are in a good

agreement with the measured one along the flexible pipe in both CF and IL direction, which demonstrates the validity of displacement reconstruction method for the flexible pipe in an oscillatory flow.

Fig. 11 and Fig. 12 show the results for the cases  $V_R = 6$  under a small

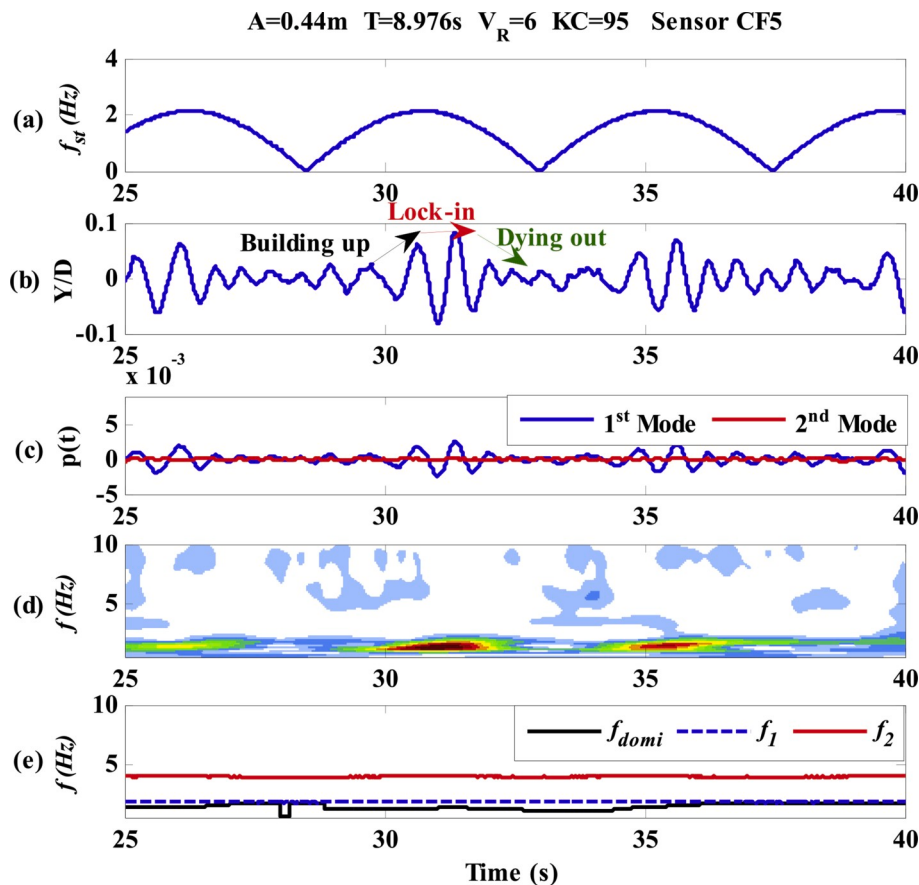


**Fig. 12.** Time history of the VIV response and time frequency distribution in the CF direction at the 5th gauge point of the straked pipe in the case of  $V_R = 6$  and  $KC = 95$ : (a) Time-varying frequency of the vortex shedding; (b) VIV displacement response; (c) Modal weight of displacement; (d) Time-varying response frequency obtained by Wavelet analysis; (e) Time-varying natural frequency and dominant response frequency.

KC number ( $KC = 30$ ) and a large KC number ( $KC = 95$ ), respectively. Each figure contains four subplots showing time history of the VIV response and time-varying frequency at the 5th gauge point of straked pipe in the CF direction. Subfigures (a) of Figs. 11 and 12 are the calculated time-varying shedding frequency  $f_{st}$  which is calculated by,

$$f_{st}(t) = \frac{St \cdot |U(t)|}{D} \quad (23)$$

where  $St$  refers to the Strouhal number,  $St = 0.2$ .  $f_{st}$  is the calculated vortex shedding frequency.

Subfigures (b) of Figs. 11 and 12 are the VIV displacement response,

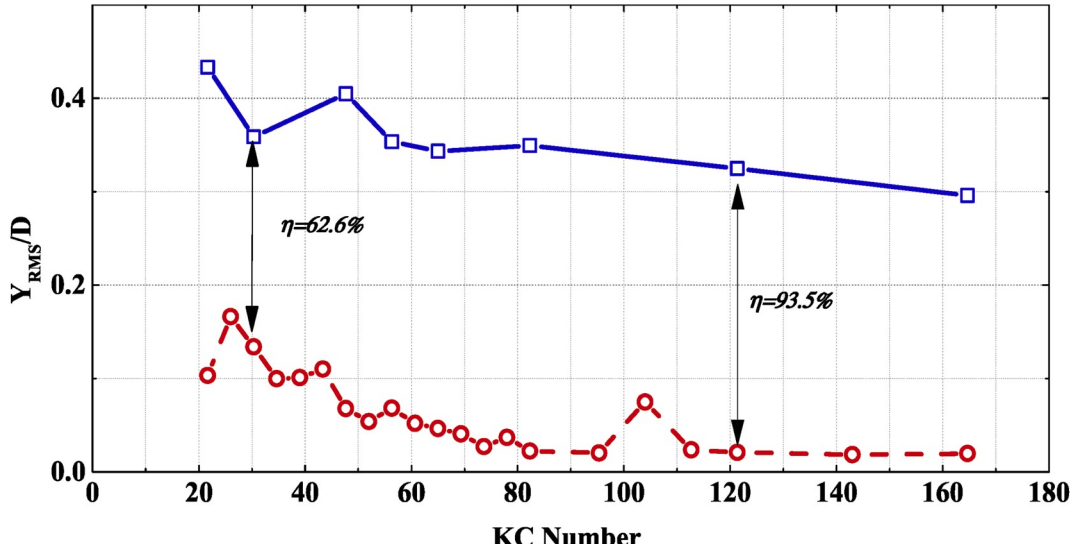


**Fig. 13.** Maximum displacement standard deviation of the VIV for the bare and straked pipes under  $V_R = 6$  (□ is the displacement response of the bare pipe; ○ is the displacement response of the straked pipe).

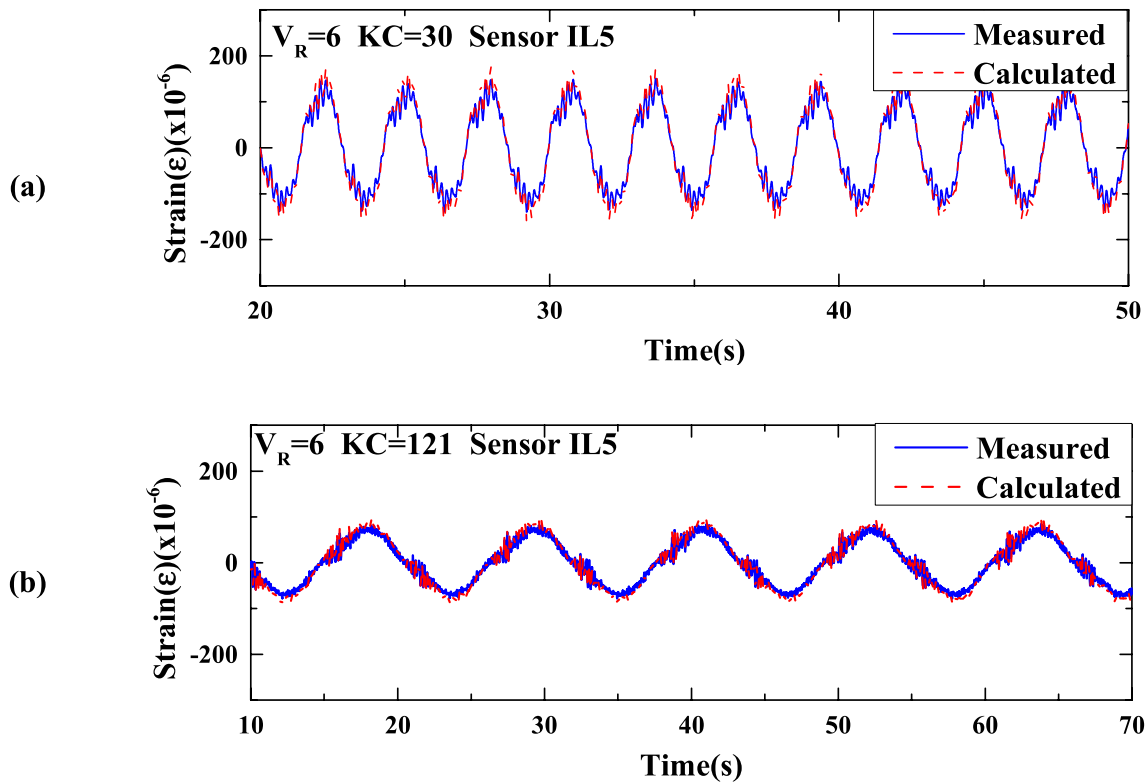


**Fig. 14.** Time histories of measured and calculated strain at position of the 5th gauge point in the case of  $V_R = 6$  for  $KC = 30$  and 121.

which is reconstructed by utilizing the modal superposition method as described in Section 3.2. Subfigures (c) of Figs. 11 and 12 show the time history of the modal weight  $p(t)$  of displacements. Subfigures (d) of Figs. 11 and 12 are the wavelet analysis of the strain signal. The depth of the color indicates the concentration level of the strain components. Subfigures (e) of Figs. 11 and 12 present the time varying natural frequency and VIV response dominant frequency. The blue dash and red solid lines represent the first and second order eigen frequency, while the black line refers to the dominant frequency. It should be noted that the first and second order eigen frequency ( $f_1, f_2$ ) have considered the measured time-varying tension  $F_T(t)$  and assuming the added mass coefficient  $C_m$  to be equal to 1, which can be calculated by

$$f_n(t) = \frac{n}{2L} \sqrt{\frac{F_T(t)}{m} + \frac{n^2 \pi^2 EI}{L^2 m}}, m = \bar{m}_s + \frac{1}{4} \pi D^2 \rho C_m (C_m = 1.0), n = 1, 2, \dots \quad (24)$$

As presented in Fig. 11, calculated shedding frequency varies from 0 to 2Hz. VIV displacement amplitude in the CF direction is less modulated and the maximum value reaches 0.25 D at  $KC = 30$ . As shown in Fig. 11 (d) and Fig. 11 (e), VIV response is always dominated by the 1st natural mode. Under larger  $KC$  number ( $KC = 95$ ) as shown in Fig. 12, a strong amplitude modulation appears and the maximum value of VIV displacement is less than 0.1 D. An obvious VIV developing process including building up, lock-in and dying out can be observed. These response features of straked pipe in an oscillatory are similar to that of the bare one (Fu et al., 2014).

Fig. 13 shows the maximum displacement standard deviation of the VIV of bare and straked pipes. The blue squares and red circles represent the displacement response of the bare and straked pipe, respectively. Although helical strakes can effectively suppress VIV response, the suppression efficiency  $\eta$  calculated by Eq. (25) at a small  $KC$  number is not very ideal as that at larger  $KC$  number (Ren et al., 2019a):

$$\eta = \frac{Y_{\max} - Y_{s\max}}{Y_{\max}} \times 100\% \quad (25)$$

$Y_{\max}$  and  $Y_{s\max}$  are the maximum root mean square values of the displacement for a bare and straked pipe, which can be obtained by Eqs. (26) and (27), respectively.

$$Y_{\max} = \max(Y_{RMS-B}(z)) \quad (26)$$

$$Y_{s\max} = \max(Y_{RMS-S}(z)) \quad (27)$$

where  $Y_{RMS-B}(z)$  and  $Y_{RMS-S}(z)$  are the RMS value of displacement response of the bare and straked pipe at the position  $z$  in the CF direction, respectively.

Recently, researchers (Chaplin et al., 2005; Song et al., 2016, 2017; Vandiver, 1985) have found that the drag forces and coefficients in the IL direction were greatly affected by the VIV response through the experiments of a flexible pipe in uniform flow. The distinctive features of VIV response between the small and large  $KC$  numbers may lead to different performance of hydrodynamic force and coefficients in the IL direction, which requires further investigation.

#### 4.2. Hydrodynamic force distribution

Based on measured strains in the IL direction, the displacement responses and hydrodynamic forces in the IL direction can be calculated. To verify this hydrodynamic force identification method, a finite element model of flexible pipe with the same parameters as those shown in Table 1 was built by ANSYS. Strain response in the IL direction was calculated by applying the same time history of identified hydrodynamic force on the flexible pipe. Fig. 14 shows the time history of measured and calculated strain at the position of the 5th gauge point in the IL direction under  $V_R = 6$  for  $KC = 30$  and 121. Compared with the measured strain, the calculated values are in a good agreement with the measured one. This consistency demonstrates the validity of this hydrodynamic identification method for a flexible pipe in an oscillatory flow.

Using the hydrodynamic force identification method proposed in Section 3.3, force at each cross section along the flexible pipe under

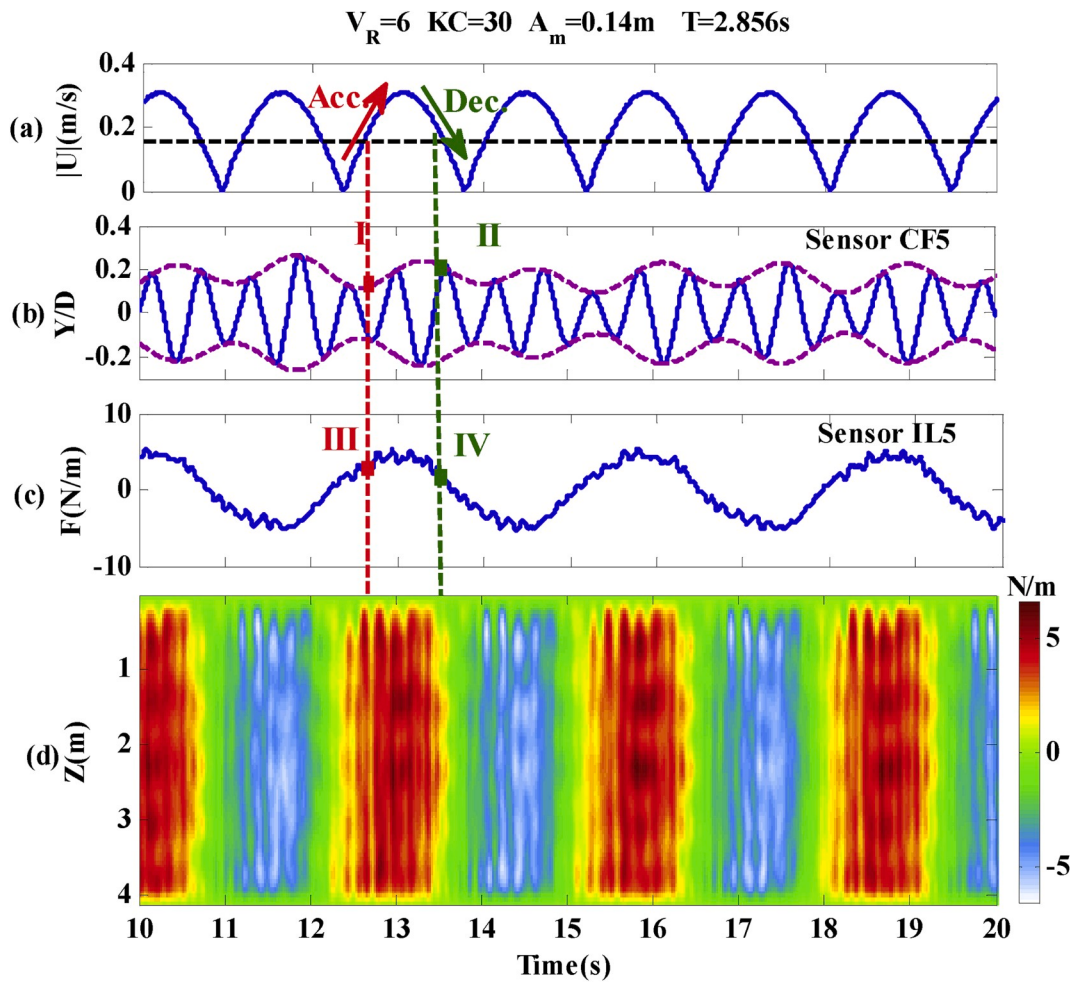


**Fig. 15.** Time histories of forced motion velocity, displacement response in the CF direction and hydrodynamic force in the IL direction at the 5th gauge point and spatiotemporal distribution of hydrodynamic force for straked pipe under  $V_R = 6.0$ ,  $KC = 30$ : (a) time history of the forced motion; (b) displacement response at the 5th gauge point in the CF direction; (c) hydrodynamic force at the 5th gauge point in the IL direction; (d) spatiotemporal distribution of hydrodynamic force in the IL direction.

different reduced velocities and KC numbers can be obtained. Fig. 15 - Fig. 18 show the time histories of forced motion velocity, displacement response in the CF direction and hydrodynamic force in the IL direction at the 5th gauge point and spatiotemporal distribution of hydrodynamic force for bare and straked pipe under  $V_R = 6.0$ . Each figure has four subplots. Figures (a) of Figs. 15–18 show time history of forced motion velocity. Figures (b) of Figs. 15–18 illustrate time history of displacement response at the 5th gauge point in CF direction. Hilbert transform method (Bracewell, 1978) is used to obtain amplitude envelope of VIV displacement response. Figures (c) of Figs. 15–18 are the time history of hydrodynamic force at the cross section of the 5th gauge point in IL direction. Figures (d) of Figs. 15–18 represent spatiotemporal distribution of hydrodynamic force in the IL direction. The gradient of the color represents the magnitude of the force. The waveforms in Figure (a), (c) and (d) of Figs. 15–18 can be clearly observed.

In an oscillatory flow, a period of the oscillation motion contains acceleration and deceleration phases. Under the small KC number ( $KC = 30$ ), as shown in Fig. 15 (b), VIV displacement response of the straked pipe at acceleration stages is not symmetric with that at deceleration stages. The amplitude value in acceleration phase at half a maximum forced motion velocity (I) is about 0.11 D and this value in deceleration phase (II) becomes 0.20 D. The former response is smaller than the latter, as called “hysteresis” (Fu et al., 2014).

However, their hydrodynamic forces behave different features. Although the asymmetric feature of displacement response is also

observed in hydrodynamic force, the force in acceleration phase is larger than that in deceleration phase. As shown in Fig. 10 (c), force is about 3.3 N/m in acceleration phase at the point (III), while about 1.4 N/m in deceleration phase at point (IV). The same phenomena can also be observed in bare pipe as presents in Fig. 17. Fig. 17 (b) shows that the VIV response reaches 0.40 D at the point (I) and 0.67 D at the point (II). Correspondingly, the forces are 1.8 N/m, 0 N/m at the points (III) and (IV), respectively.

The main reasons for this interesting phenomenon will be further analyzed below. Compared with the straked pipe, the higher frequency components of hydrodynamic force on the bare pipe fluctuates more obviously. It indicates that helical strake can effectively reduce this higher frequency force fluctuation. The reasons can be attributed to the suppression effects of helical strakes on VIV response in the CF direction. This is consistent with results derived from experiments in uniform flow (API, 1998; Ren et al., 2019b).

Under large KC number ( $KC = 121$ ), VIV response cannot be induced by the disorder and weak vortex due to the vortex-breaking effects of helical strakes (Ren et al., 2019a) as shown in Fig. 17 (a). The VIV developing process cannot be clearly observed at this case. The response amplitudes at points (I) and (II) are 0.03 D and 0.014 D, respectively. The VIV response hysteresis is not obvious under this KC number. The force at points (III) and (IV) are 1.9 N/m and 0.8 N/m. For the bare pipe, VIV developing process and hysteresis can be clearly seen at  $KC = 121$  as shown in Fig. 18 (b). The VIV response amplitudes at points (I) and (II)

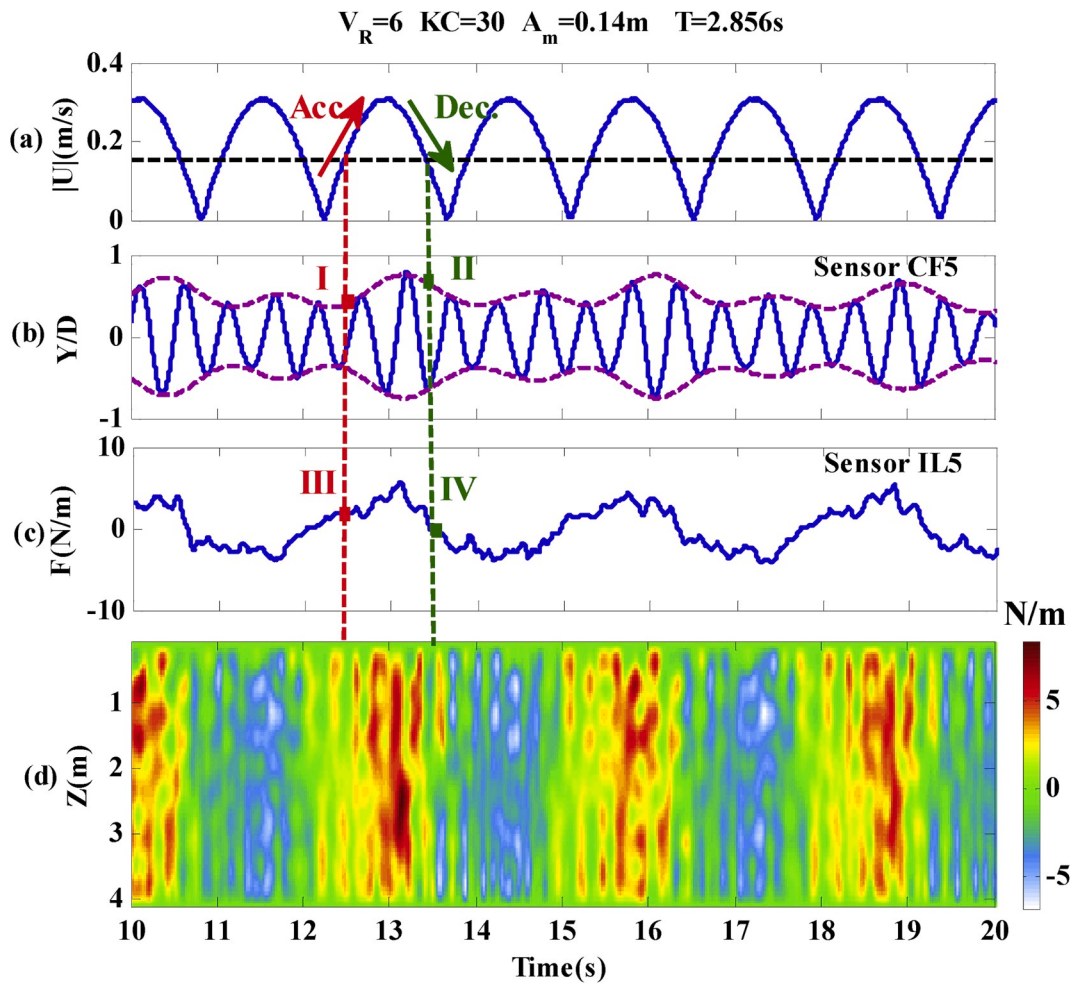


**Fig. 16.** Time histories of forced motion velocity, displacement response in the CF direction and hydrodynamic force in the IL direction at the 5th gauge point and spatiotemporal distribution of hydrodynamic force for bare pipe under  $V_R = 6.0$ ,  $KC = 30$ : (a) time history of the forced motion; (b) displacement response at the 5th gauge point in the CF direction; (c) hydrodynamic force at the 5th gauge point in the IL direction; (d) spatiotemporal distribution of hydrodynamic force in the IL direction.

are  $0.25 D$  and  $0.53 D$ , respectively. Corresponding forces at points (III) and (IV) are  $1.3 \text{ N/m}$  and  $1.0 \text{ N/m}$ . Similar with the case of small KC number, fluctuation of hydrodynamic force on the bare pipe is more obvious than the straked pipe.

These observations indicate that the asymmetric features of VIV response and hydrodynamic force are the main phenomena for both bare and straked pipes. To further illustrate these features more clearly,  $Y/D$ ,  $F$  versus instantaneous reduced velocity  $|U|/(f_1 * D)$  are plotted in Fig. 19 and Fig. 20. The red and green solid lines represent corresponding response and force at acceleration and deceleration stages, respectively. Differences between the red and green lines in both Figs. 19 and 20 indicate that both the straked and bare pipe in oscillatory flow for these KC numbers have different VIV response features at acceleration and deceleration stages; i.e., ‘hysteresis’ phenomenon (Fu et al., 2014).

This is caused by the lag between vortex shedding and instantaneous reduced velocity. The vortex shedding doesn't change immediately with forced motion velocity altering (Fu et al., 2018). However, at large KC number, forced motion period and displacement become longer and larger. The vortex will be breaking by helical strakes. When KC number reaches a certain large value, vortex-induced vibration is difficult to be excited. Both development process and hysteresis of vortex-induced vibration are difficult to be clearly observed.

Different from VIV response with instantaneous reduced velocity, the force in acceleration phase are larger than that in deceleration phase. It is not consistent with the belief that the larger VIV response will lead to

larger drag force based on the experimental results of flexible pipe in steady flow (Chaplin et al., 2005; Ren et al., 2019b; Vandiver, 1985). These unexpected results may be closely related to the interaction between the fluids derived forth and the backward motion of the flexible pipe.

Fig. 21 presents the sketch of this interaction. In the deceleration phase, the pipe drives the attached water to the right. When pipe accelerates back to the left, it will encounter former water body moving to the right. This makes the effective velocity in acceleration phase faster than that in deceleration phase, resulting in corresponding former hydrodynamic force is larger than the latter one. This is called “wake effects” (Williamson, 2006). Although helical strakes reduced higher frequency hydrodynamic force fluctuation through suppressing VIV response, the asymmetric features of the force cannot be avoided. More insightful experiments and CFD simulations would be carried out in the near future to further investigate this interesting phenomenon.

#### 4.3. Drag and added mass coefficients

After obtaining displacement response and hydrodynamic force in the IL direction, the drag coefficient  $C_D(z)$  and added mass coefficient  $C_m(z)$  at each node of bare and straked pipe can be identified through the proposed method in Section 3.3. Fig. 22 illustrates the distribution of drag coefficients along bare and straked pipes under  $V_R = 6.0$  for  $KC = 30$  and 121. Fig. 22 (a) shows drag coefficients of the straked pipe are

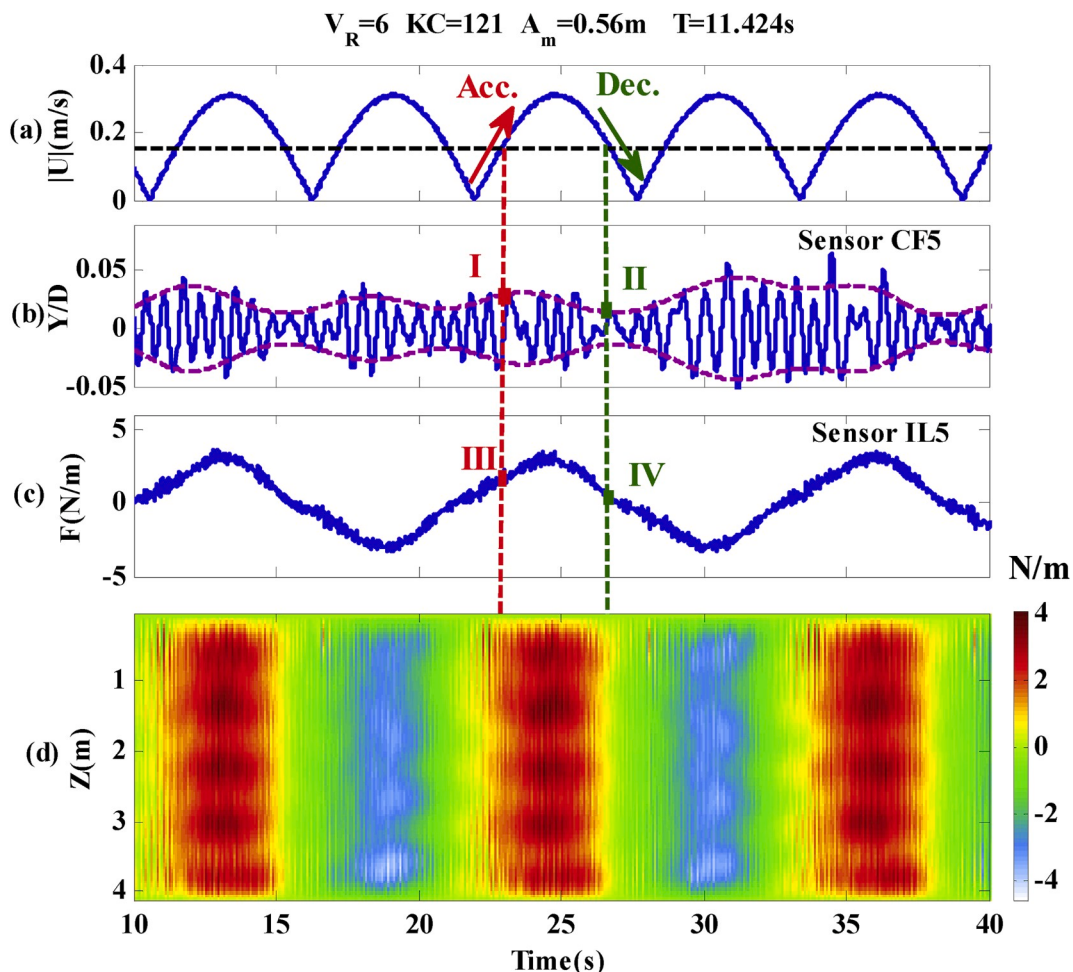


**Fig. 17.** Time histories of forced motion velocity, displacement response in the CF direction and hydrodynamic force in the IL direction at the 5th gauge point and spatiotemporal distribution of hydrodynamic force for straked pipe under  $V_R = 6.0$ ,  $KC = 121$ : (a) time history of the forced motion; (b) displacement response at the 5th gauge point in the CF direction; (c) hydrodynamic force at the 5th gauge point in the IL direction; (d) spatiotemporal distribution of hydrodynamic force in the IL direction.

larger than that of the bare pipe.  $C_D$  are around 2.3 and 3.2 for the bare and straked pipes, respectively. Although the VIV response of the straked pipe is not as significant as that of the bare one, magnification effects of helical strake on drag coefficients can be clearly found.

With KC number increasing from 30 to 121, all  $C_D$  of both the straked and bare pipes are all approaching asymptotically to 1.90. Compared with the typical value  $C_D = 1.2$  derived from the towing test of stationary rigid cylinder (Blevins and Saunders, 1977), drag of both the bare and straked pipes are all amplified. However, the reasons of drag amplification mechanism are different in an oscillatory flow: for the bare pipe, drag force is amplified by VIV response; for the straked pipe, it is caused by an increased hydrodynamic diameter and altered wake (Ren et al., 2019b). Unexpectedly, two drag coefficients of the bare and straked pipes under a larger KC number are at the same level. It can be also concluded that the magnified effects on drag by increasing hydrodynamic diameter for the straked pipe is not always necessarily greater than that of VIV response in the CF direction for the bare pipe in oscillatory flow with a larger KC number.

Fig. 23 presents the distribution of added mass coefficients along the bare and straked pipes.  $C_m$  of the straked pipe is obviously larger than that of bare pipe in all cases. It is consistent with the results of API (1998) (API, 1998). To validate the reliability of identified coefficients, the coefficients are used to calculate the corresponding hydrodynamic forces. Fig. 24 shows the time history of measured and calculated hydrodynamic force on straked pipe in the IL direction in the case of  $V_R =$

6.0 for  $KC = 30$ . The blue solid line and red dash line represent the measured and calculated force, respectively. A good agreement is seen between these two values at different positions along the flexible pipe. This demonstrates that the identified coefficients are correct.

To further reveal the effects of helical strake on force coefficients in the IL direction, the mean coefficients are introduced here. The mean drag coefficients  $\bar{C}_D$  and mean added mass coefficients  $\bar{C}_m$  are defined as,

$$\bar{C}_D = \frac{1}{L} \int_0^L C_D(z) dz \quad (28)$$

$$\bar{C}_m = \frac{1}{L} \int_0^L C_m(z) dz \quad (29)$$

where  $L$  is the length of the flexible pipe model. Through Eqs. (28) and (29), mean drag and added mass coefficients under different KC numbers and maximum reduced velocities are summarized in Fig. 25 and Fig. 28.

As shown in Fig. 25, the red circle and blue rectangle symbols represent the mean drag coefficients on the straked and bare pipe, respectively. It shows that drag coefficients on both the bare and straked pipes under small KC number are magnified, while distributions of mean drag coefficient are stable with KC number under larger KC number. More in detail, under small KC number, the amplified phenomena of drag coefficients on the straked pipe are more significant than the bare one.

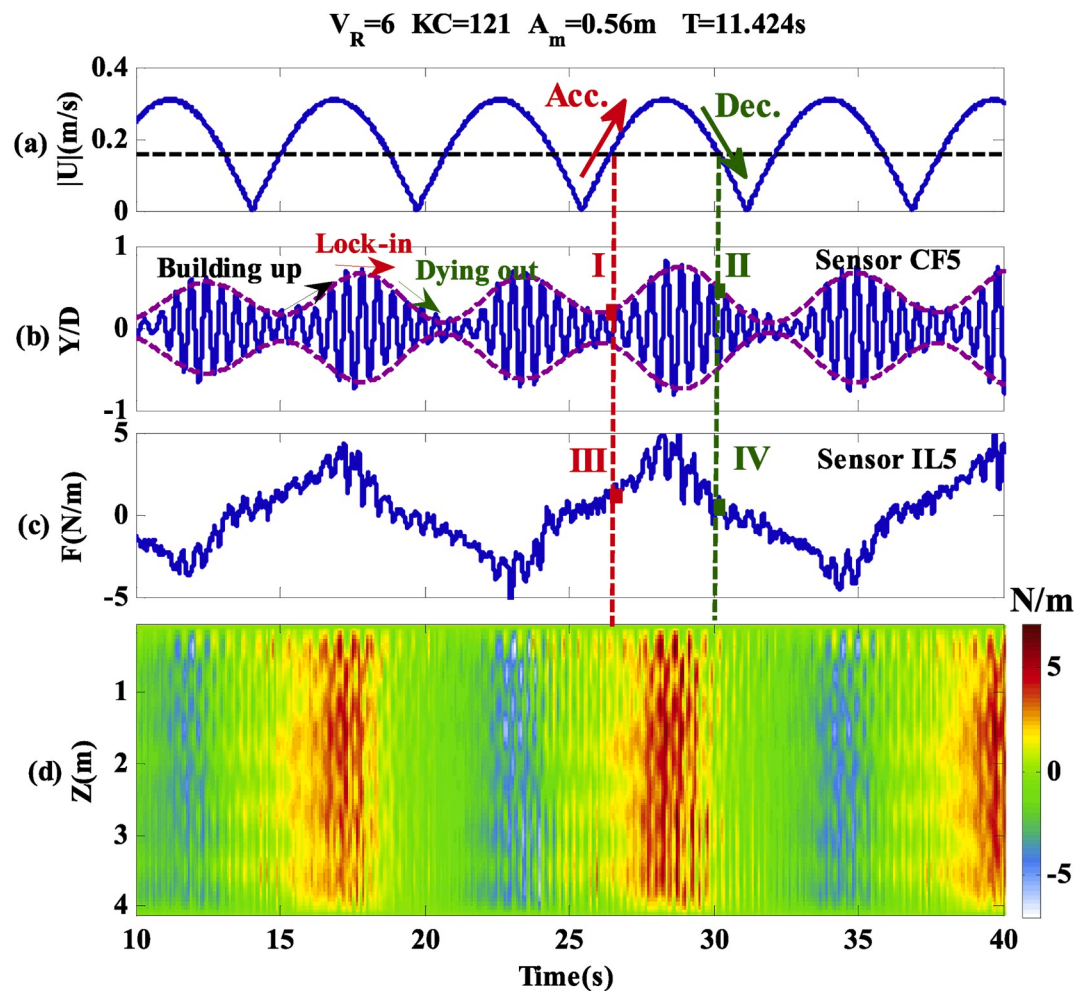


**Fig. 18.** Time histories of forced motion velocity, displacement response in the CF direction and hydrodynamic force in the IL direction at the 5th gauge point and spatiotemporal distribution of hydrodynamic force for bare pipe under  $V_R = 6.0$ ,  $KC = 121$ : (a) time history of the forced motion; (b) displacement response at the 5th gauge point in the CF direction; (c) hydrodynamic force at the 5th gauge point in the IL direction; (d) spatiotemporal distribution of hydrodynamic force in the IL direction.

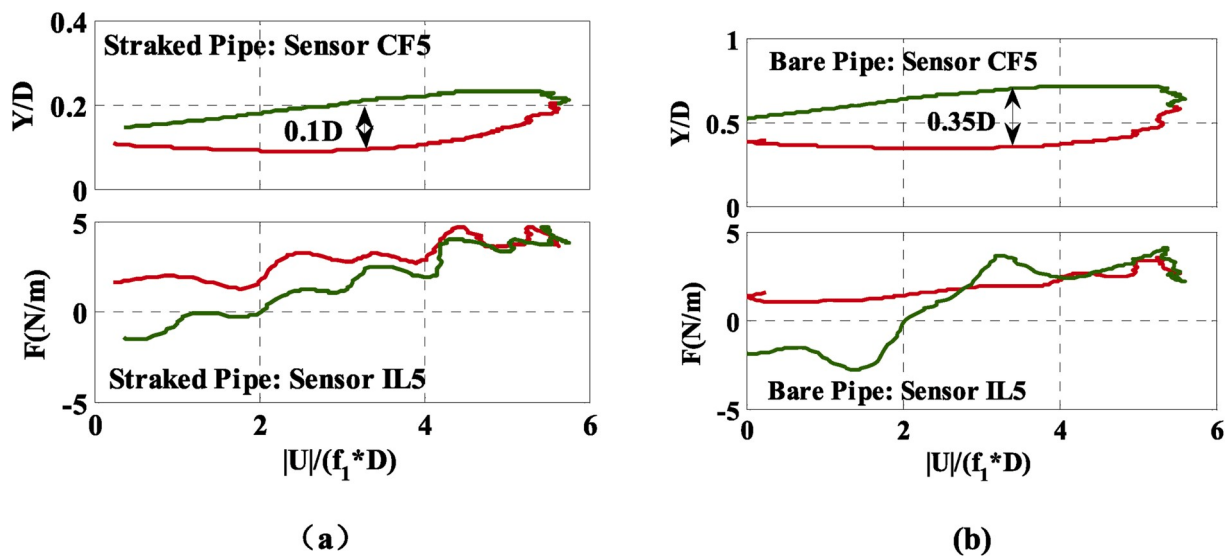


**Fig. 19.** Hysteresis of VIV response and hydrodynamic force asymmetry for  $V_R = 6$  and  $KC = 30$ .

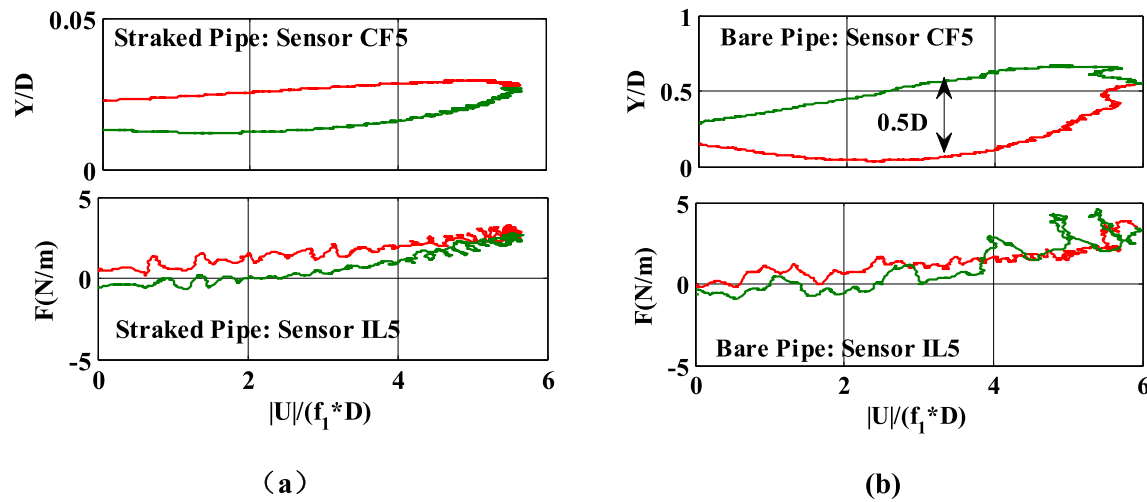


Fig. 20. Hysteresis of VIV response and hydrodynamic force asymmetry for  $V_R = 6$  and  $KC = 121$ .

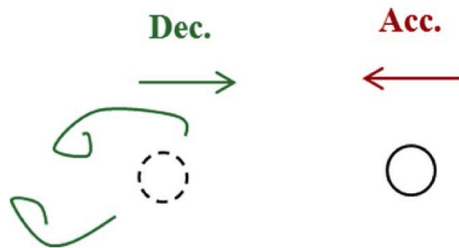


Fig. 21. Sketch of interaction between the fluids derived forth and backward motion of the flexible pipe.

Fig. 25 (a) presents mean drag coefficients of the straked pipe reach 4.1, while 3.3 for bare pipe under  $V_R = 4.0$  and  $KC = 13$ . As reduced velocities increases to 6 and 8,  $\bar{C}_D$  of staked pipe can be amplified to approximately 5.8 and 8.8 as illustrated in Fig. 25 (b) and (c) under  $KC = 13$  and 9, respectively. Under larger KC number, the mean drag coefficients are approaching to 1.8 and 1.5 for bare and straked pipe as shown in Fig. 25 (a) under  $V_R = 4.0$ , respectively; and  $\bar{C}_D$  stabilize at 1.9 and 2.0 for both the bare and straked pipes as  $V_R$  increases to 6.0 and 8.0 as shown in Fig. 25 (b) and (c), respectively. The mean drag coefficients for both bare and straked pipe increase with maximum reduced velocities under a larger KC number.

To further reveal the reasons behinds the above features of mean drag coefficients and investigate the effects of helical strakes and VIV

responses on drag coefficients, VIV displacement amplitudes are summarized in Fig. 26. Under  $V_R = 4.0$ , the response of bare one is only excited under small KC number and correspondingly magnification of drag coefficients can be also seen. As KC number increases, VIV decreases to stable value, which is less than 0.1 D. Meanwhile, mean drag coefficients decrease from 3.3 at  $KC = 13$  to a smaller asymptotic value 1.5 at larger KC number. These two value trends have good consistency.

As a result, drag amplification can be attributed to the VIV response as the results reported by Vandiver et al. (1985) according to experiments of a flexible pipe in steady flow. Compared with the bare pipe, VIV responses of the straked pipe are sufficiently suppressed, while amplification of drag coefficients of the straked pipe can be still seen at the same magnitude with the bare one under a small KC number. The magnification of drag on straked pipe is even slightly obvious. The downward trend can also be seen in mean drag coefficients with KC number. Therefore, it can be easily inferred that drag magnification of the straked pipe in an oscillatory flow is not caused by VIV response in the CF direction.

The main reasons can be attributed to the “wake effect” as previously mentioned. In the case of a small KC number, the forced oscillation period is shorter and the forced oscillation amplitude is smaller. The time of the pipe in the wake is more pronounced. The effective velocity will be larger than the actually forced oscillation velocity in most time of the whole oscillation period. When the KC number increase, the wake effects will be weakened. Thus, although there is no obvious VIV response, the drag coefficients of the straked pipe are significantly magnified at small KC number and decrease to the asymptotic value at a

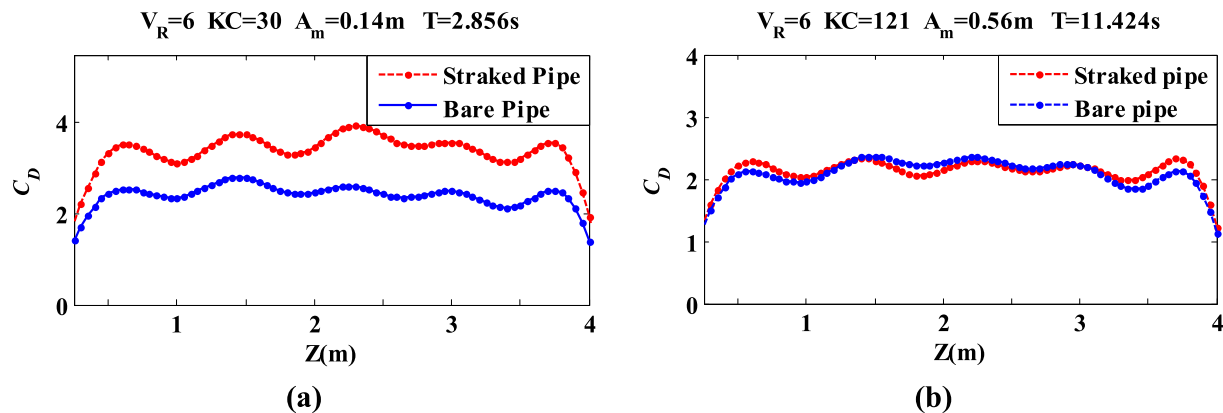


Fig. 22. Distributions of drag coefficients along bare and straked pipe in the case of  $V_R = 6.0$  for  $KC = 30$  and 121.

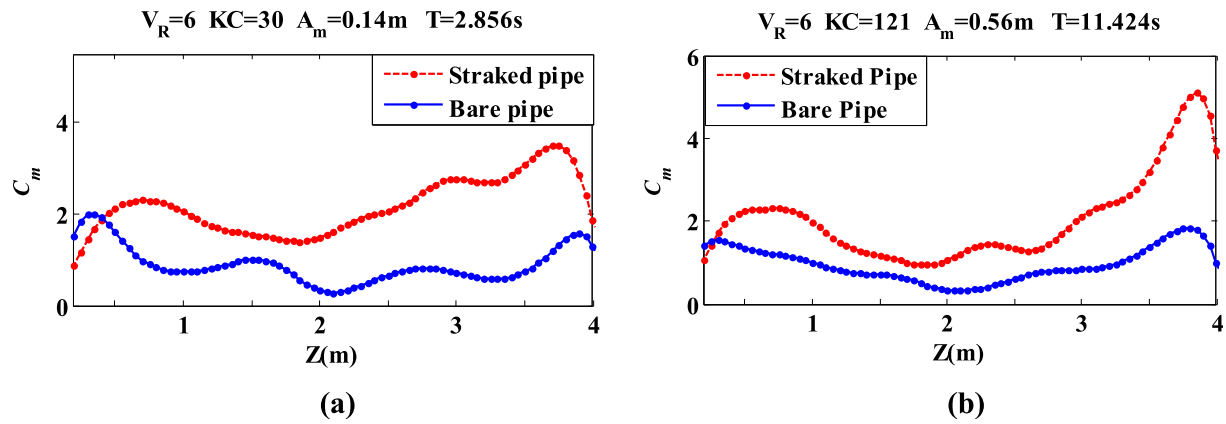


Fig. 23. Distributions of added mass coefficients along bare and straked pipe in the case of  $VR = 6.0$  for  $KC = 30$  and  $121$ .

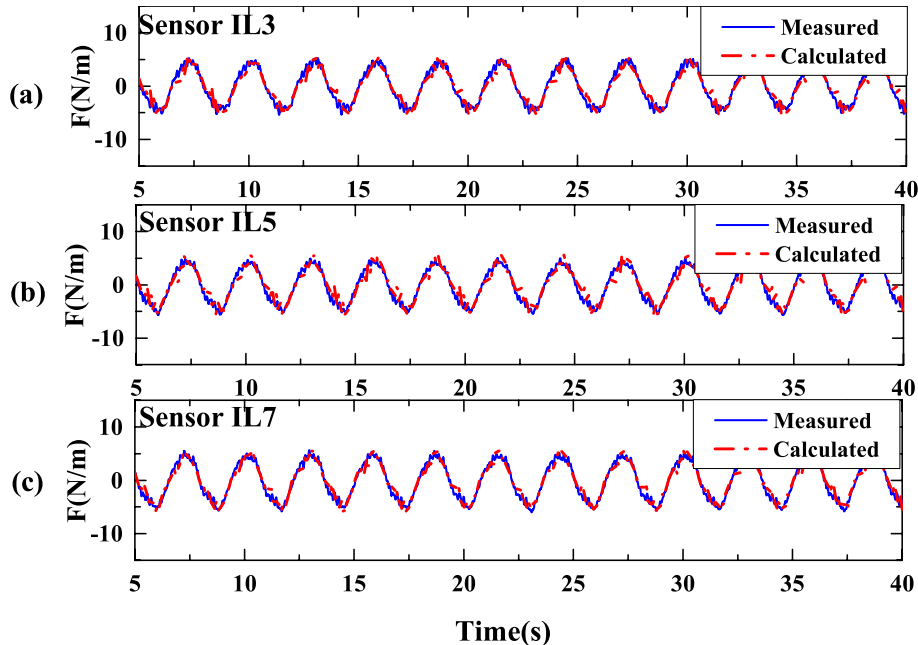


Fig. 24. Time history of measured and calculated hydrodynamic force on the straked pipe in the IL direction in the case of  $VR = 6.0$  for  $KC = 30$ .

larger  $KC$  number. Beyond that, slightly larger coefficients observed on straked pipe can be attributed to this hydrodynamic diameter increased due to covered helical stakes.

As maximum reduced velocities increase to 6 and 8, VIV of bare pipe is significantly excited in the case of all  $KC$  numbers. Maximum VIV displacement amplitudes increase with maximum reduced velocities. Mean values of VIV displacement amplitudes are around  $0.15 D$ ,  $0.35 D$  and  $0.45 D$  for  $V_R = 4$ ,  $6$  and  $8$ , respectively. Correspondingly, increased trends of  $\bar{C}_D$  are also seen. This is consistent with the belief that larger VIV response leads to larger drag force by broadening incoming flow area as previously described.

However, the considerable VIV of straked pipe only occurs in the case of small  $KC$  number ( $KC$  is around 30). We surprisingly find that the maximum drag coefficients of straked pipe do not appear when VIV responses reach their maximum value. Although the VIV response at  $KC < 20$  is smaller than that at  $KC$  around 30,  $\bar{C}_D$  of the former one is significantly larger than the latter. So VIV response of the straked pipe is not a direct reason for the drag magnification under small  $KC$  number.

Another factors as wake effect and increasing hydrodynamic diameter by helical stakes may play the dominant role. It also indicates that drag magnification of helical stakes caused by "wake effects" is more

significant than VIV in the case of small  $KC$  number. Compared with the bare pipe, even though obvious VIV of the bare pipe is excited, the drag coefficients of the bare pipe are not at the same magnitude as those of straked pipe. This means the effects of wake on the straked pipe is more intensive than the bare pipe and further indicates that the helical stakes can enhance the effects of wake.

To better understand the enhanced effects of helical stakes on flow wake, the sketches are shown in Fig. 27. Due to the viscosity of fluid, water attached to a flexible pipe are driven by the movement of pipe. When the pipe decelerates and moves in the opposite direction, the movement direction of water body cannot change immediately, resulting in the effective velocity greater than the actual velocity as shown in Fig. 27 (a). Different from bare pipe, helical stakes tied on flexible pipe make the attached water hardly escape. This allows a larger volume of added fluid to be fully accelerated and finally enhanced the above effects of wake as presented in Fig. 27 (b). Under  $V_R = 6$  and  $8$  in the case of larger  $KC$  number, two drag coefficients are the same. It means the amplification of drag coefficient caused by VIV for the bare pipe is equal to that by increasing hydrodynamic diameter and enhanced effects of flow wake for the straked pipe in the case of larger  $KC$  number in an oscillatory flow.

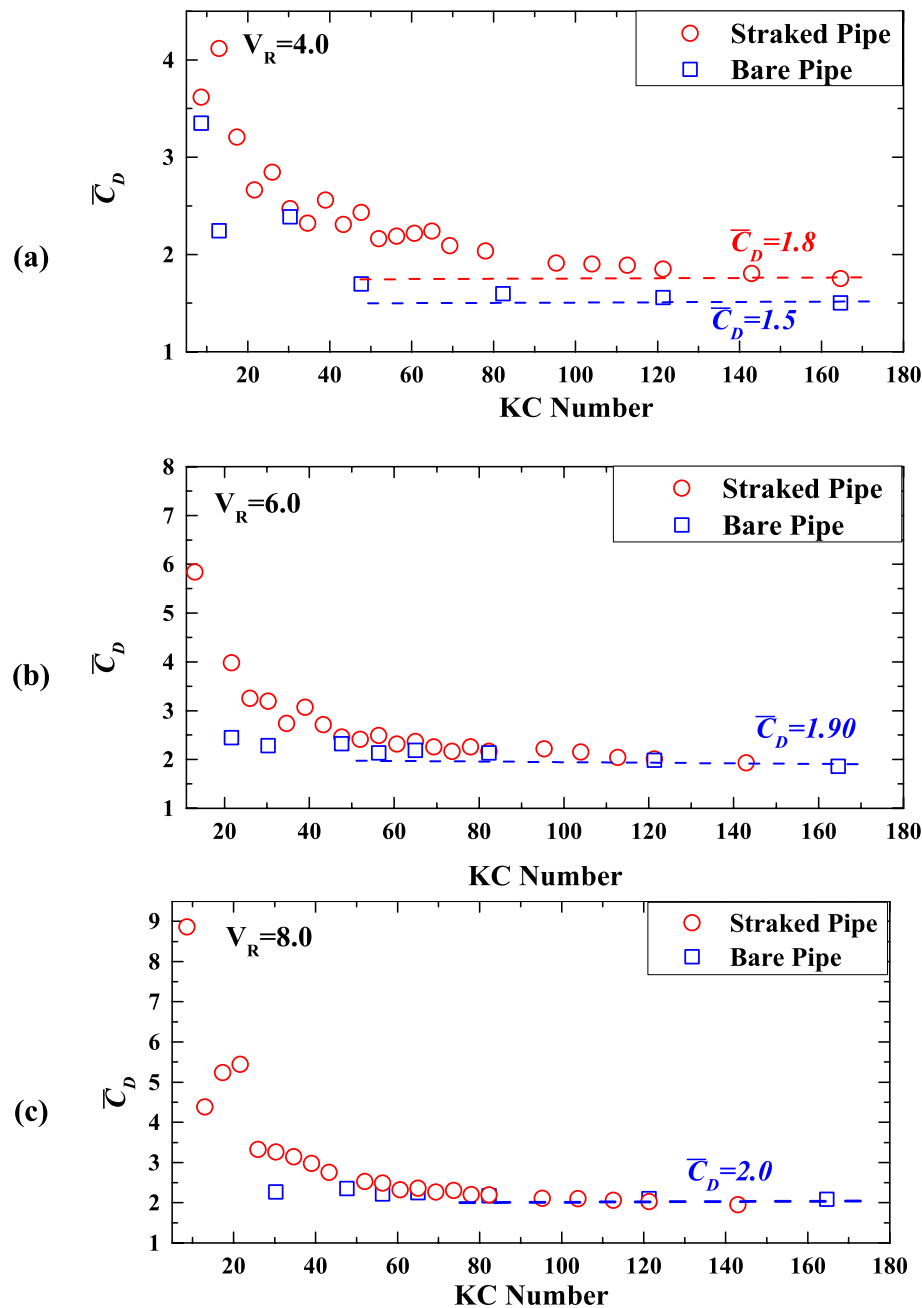


Fig. 25. Distributions of drag coefficients versus KC numbers under different reduced velocities.

Fig. 28 shows the distribution of added mass coefficients versus KC number under different maximum reduced velocities. For the bare pipe, there are no obvious differences in the added mass coefficients among various maximum reduced velocities. The values of  $\bar{C}_m$  for the bare pipe are approaching asymptotically to approximately 0.8. While the distributions of mean added mass of streaked one under different maximum reduced velocities are more discrete and obviously amplified. The mean added mass of straked pipe is around 0.8, 2.0 and 3.0 under  $V_R = 4.0, 6.0$  and 8.0, respectively.

The magnification of added mass coefficients can be also attributed to helical strakes impeding the detachment of attaching water. The larger added mass coefficients indicate that much more water attached to the straked pipe. Under lower reduced velocity, the force oscillation period is too long and attached water can easily detach from helical strakes. However, when oscillation period becomes shorter and the maximum reduced velocities increase to 6.0 and 8.0, it will be more

difficult for attached water to escape. Thus, the added mass coefficients increase with  $V_R$ . These results are consistent with the above explanations of the enhanced effects of helical strakes on wake as previously mentioned.

In the past research, the vortex-induced vibration suppression efficiency of the helical strakes, 15 D in pitch and 0.25 D in height, was tested in a rigid cylinder experiments under steady flow by Schaudt et al. (2008), obtaining at least 94% reduction. Moreover, the drag coefficients are found to be approximately 1.5 in the steady flow, which is not very amplified by helical strakes. It means the 15D/0.25D helical strakes can serve as an ideal suppression device of the VIV in the steady flow.

However, through above observed results in the present work, the application of helical strakes may cause great concern in an oscillatory flow. Such a large coefficient of straked pipe under small KC number in an oscillatory flow is previously unimaginable in riser design when using

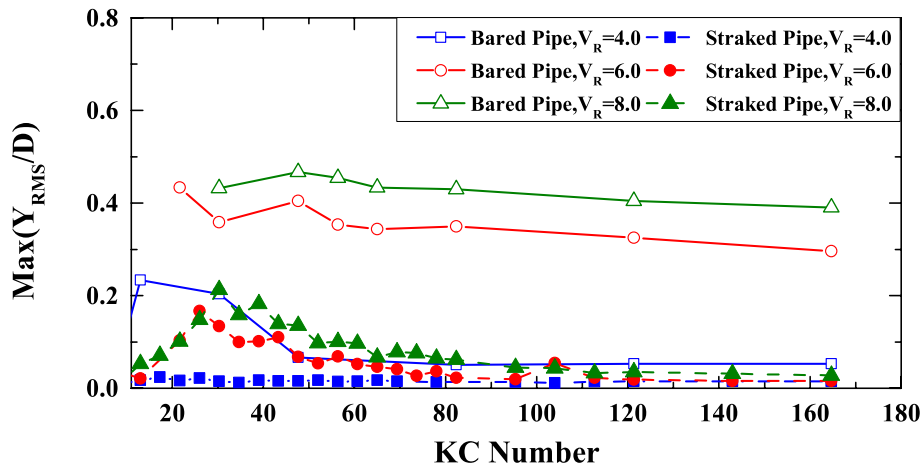


Fig. 26. Maximum root mean square VIV displacement responses versus KC numbers under different reduced velocities.

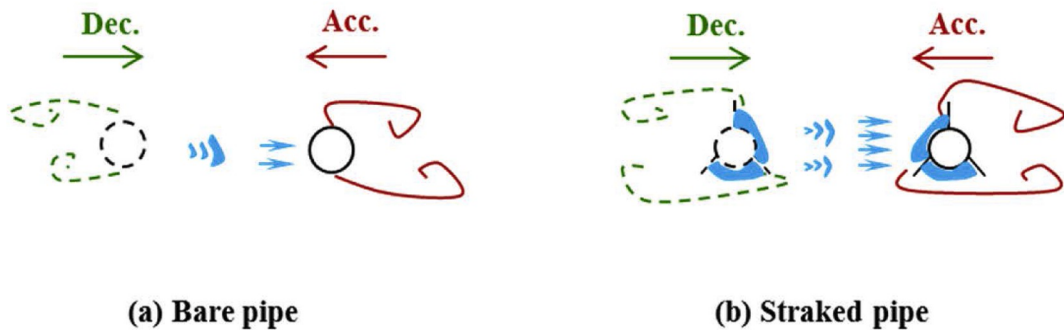


Fig. 27. Sketches of enhanced effects of helical strakes on flow wake.

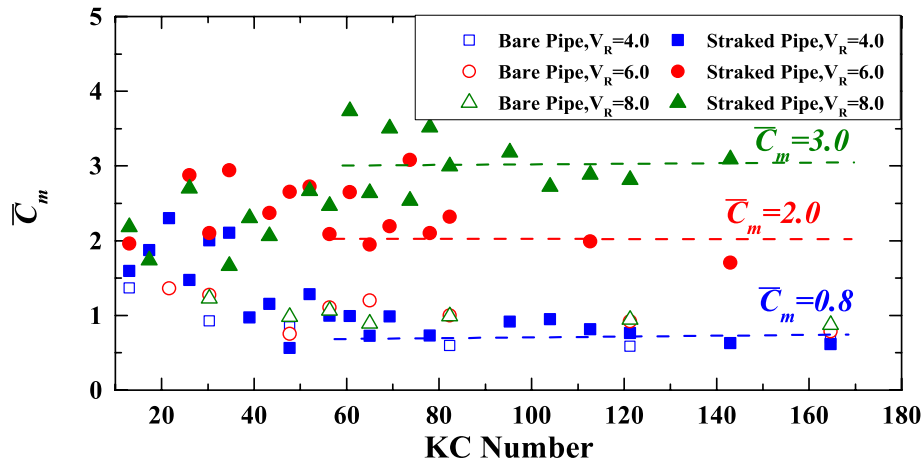


Fig. 28. Distributions of added mass coefficients versus KC numbers under different reduced velocities.

the helical strakes to suppress VIV issue. Beyond that, the suppression efficiency of helical strakes is not ideal as that in steady flow under small KC number (KC around 30) as shown in Fig. 26. Therefore, lower suppression efficiency and severe drag magnification effects of helical strakes may have an extremely adverse influence on riser. This may lead to serious potential engineering safety problems and must be taken into consideration in real project. It suggests that suppression efficiency and drag amplification for helical strakes with other pitches and heights should be evaluated through flexible pipe experiments not only in a steady flow but also in an oscillatory flow.

## 5. Conclusions

In this paper, magnification of hydrodynamic coefficients of a straked pipe in an oscillatory flow including drag and added mass coefficients are experimentally investigated. The maximum reduced velocities range from 4 to 8, and the KC numbers vary between 9 and 165. The hydrodynamic force and coefficients on helical strakes are first revealed by using inverse analysis and the least squares method. The features of hydrodynamic force in deceleration and acceleration phase are presented in detail. Distribution of corresponding mean coefficients versus KC numbers and maximum reduced velocities are summarized.

Compared with a bare pipe, effects of helical strakes covering on flexible pipe on hydrodynamic coefficients are further investigated. The main conclusions are as follows:

- (1) Asymmetric features of hydrodynamic force caused by “wake effects” are first observed in both bare and straked pipes. Moreover, helical strakes can effectively reduce higher frequency hydrodynamic force fluctuation through suppressing VIV response.
- (2) Under large KC number, the drag coefficients of the straked pipe are at the same level as the bare one, while added mass coefficients of the former one are larger than that of the latter one. Magnified effects on drag by increasing hydrodynamic diameter for straked pipe are not always necessarily greater than that of VIV response in the CF direction for the bare pipe in an oscillatory flow.
- (3) Under small KC number, significantly amplification was found in the straked pipe. The maximum value of  $\bar{C}_D$  can reach approximately 10. Enhanced effects on the wake and increasing hydrodynamic diameters by helical strakes are main potential reasons.
- (4) Lower suppression efficiency and severe drag magnification effects of helical strakes under small KC number may have an extremely adverse influence on riser. It may lead to serious potential engineering safety problems and must be taken into consideration in a real project.

#### Declaration of competing interest

The authors declare that they have no known competing financial interests or personal relationships that could have appeared to influence the work reported in this paper.

#### CRediT authorship contribution statement

**Haojie Ren:** Writing - original draft, Investigation, Formal analysis. **Mengmeng Zhang:** Investigation. **Jingyun Cheng:** Investigation. **Peimin Cao:** Investigation. **Yuwang Xu:** Investigation. **Shixiao Fu:** Investigation, Formal analysis. **Chang Liu:** Investigation. **Yifan Wang:** Investigation.

#### Acknowledgments

The authors gratefully acknowledge the support from the National Science Fund for Distinguished Young Scholars of China (No. 51825903), National Natural Science Foundation of China (No. 51909159), Joint Funds of the National Natural Science Foundation of China (U19B2013), Shanghai Science and Technology Program (No. 19XD1402000, No. 19JC1412800, 19JC1412801), Key projects for intergovernmental cooperation in international science, technology and innovation(SQ2018YFE010801), The 13th Five-Year National Science and Technology Major Project of China (No. 2016ZX05028-001). All of the authors also would like to acknowledge support and permission from SBM Offshore to prepare and publish this work.

#### References

- Allen, D.W., Henning, D.L., Li, L., 2006. High Reynolds Number Flow Tests of Flexible Cylinders with Helical Strakes, International Conference on Offshore Mechanics and Arctic Engineering, pp. 359–367.
- API, 1998. Recommended Practice API-RP-2rd: Design of Risers for Floating Production Systems (FPSs) and Tension Leg Platforms (TLPs). American Petroleum Institute, Washington,D.C., USA, 1998.
- Bearman, P.W., Downie, M.J., Graham, J.M.R., Obasaju, E.D., 1985. Forces on cylinders in viscous oscillatory flow at low Keulegan-Carpenter numbers. *J. Fluid Mech.* 154 (154), 337–356.
- Blevins, R.D., Saunders, H., 1977. Flow-induced Vibration. Van Nostrand Reinhold Co.
- Bracewell, R.N., 1978. The Fourier Transform and its Applications. McGraw-Hill, New York, pp. 267–274.
- Chaplin, J.R., Bearman, P.W., Huarte, F.J.H., Pattenden, R.J., 2005. Laboratory measurements of vortex-induced vibrations of a vertical tension riser in a stepped current. *J. Fluid Struct.* 21 (1), 3–24.
- Cheng, J., Cao, P., Fu, S., Constantinides, Y., 2016. Experimental and Numerical Study of Steel Lazy Wave Riser Response in Extreme Environment, ASME 2016 International Conference on Ocean, Offshore and Arctic Engineering. V005T004A055.
- Constantinides, Y., Cao, P., Cheng, J., Fu, S., Kusinski, G., 2016. Steel Lazy Wave Riser Tests in Harsh Offshore Environment, ASME 2016 International Conference on Ocean, Offshore and Arctic Engineering. V005T004A057.
- Fu, S., Wang, J., Baarholm, R., Wu, J., Larsen, C.M., 2014. Features of vortex-induced vibration in oscillatory flow. *J. Offshore Mech. Arctic Eng.* 136 (1), 011801.
- Fu, B., Zou, L., Wan, D., 2018. Numerical study of vortex-induced vibrations of a flexible cylinder in an oscillatory flow. *J. Fluid Struct.* 77, 170–181.
- Galvao, R., Lee, E., Farrell, D., Hover, F., Triantafyllou, M., Kitney, N., Beynet, P., 2008. Flow control in flow-structure interaction. *J. Fluid Struct.* 24 (8), 1216–1226.
- Gao, Y., Fu, S., Ma, L., Chen, Y., 2016. Experimental investigation of the response performance of VIV on a flexible riser with helical strakes. *Ships Offshore Struct.* 11 (2), 113–128.
- Gao, Y., Fu, S., Ren, T., Xiong, Y., Song, L., 2015. VIV response of a long flexible riser fitted with strakes in uniform and linearly sheared currents. *Appl. Ocean Res.* 52, 102–114.
- He, J.W., Glowinski, R., Metcalfe, R., Nordlander, A., Periaux, J., 2000. Active control and drag optimization for flow past a circular cylinder  $\star$ : I. Oscillatory cylinder rotation. *J. Comput. Phys.* 163 (1), 83–117.
- Schadt, J.K., Wajnlonis, C., Spencer, D., Xu, J., 2008. Benchmarking of VIV Suppression Systems. Schadt, Kenneth J., et al. “Benchmarking of VIV Suppression Systems.” Asme International Conference on Offshore Mechanics & Arctic Engineering. <https://doi.org/10.1115/OMAE2008-57065>.
- Jeon, S., Choi, J., Jeon, W., Choi, H., Park, J., 2004. Active Control of Flow over a Sphere for Drag Reduction at a Subcritical Reynolds Number. Cambridge University Press ([etc.]).
- Korkischko, I., Meneghini, J.R., Gioria, R.S., Jabardo, P.J., Casaprina, E., Franciss, R., 2007. An Experimental Investigation of the Flow Around Straked Cylinders, ASME 2007 International Conference on Offshore Mechanics and Arctic Engineering, pp. 641–647.
- Lie, H., Kaasen, K.E., 2006. Modal analysis of measurements from a large-scale VIV model test of a riser in linearly sheared flow. *J. Fluid Struct.* 22 (4), 557–575.
- Morison, J.R., Johnson, J.W., O'Brien, M.P., 1953. Experimental studies of forces on piles. *Coastal Engineering Proceedings* 1, 1–31.
- Morison, J.R., Johnson, J.W., Schaaf, S.A., 1950. The force exerted by surface waves on piles. *J. Petrol. Technol.* 2 (5), 149–154.
- Pesce, C.P., Franzini, G.R., Fujarra, A.L.C., Gonçalves, R.T., Salles, R., Mendes, P., 2017. Further Experimental Investigations on Vortex Self-Induced Vibrations (VSIV) with a Small-Scale Catenary Riser Model. (S57649). V002T008A016.
- Quen, L.K., Abu, A., Kato, N., Muhamad, P., Sahekhaini, A., Abdullah, H., 2014. Investigation on the effectiveness of helical strakes in suppressing VIV of flexible riser. *Appl. Ocean Res.* 44 (3), 82–91.
- Ren, H., Xu, Y., Cheng, J., Cao, P., Zhang, M., Fu, S., Zhu, Z., 2019a. Vortex-induced vibration of flexible pipe fitted with helical strakes in oscillatory flow. *Ocean Eng.* 189, 106274.
- Ren, H., Xu, Y., Zhang, M., Fu, S., Meng, Y., Huang, C., 2019b. Distribution of drag coefficients along a flexible pipe with helical strakes in uniform flow. *Ocean Eng.* 184, 216–226.
- Song, L., Fu, S., Dai, S., Zhang, M., Chen, Y., 2016. Distribution of drag force coefficient along a flexible riser undergoing VIV in sheared flow. *Ocean Eng.* 126, 1–11.
- Song, L., Fu, S., Li, M., Gao, Y., Ma, L., 2017. Tension and drag forces of flexible risers undergoing vortex-induced vibration. *China Ocean Eng.* 31 (1), 1–10.
- Sumer, B.M., Fredsøe, J., 1988. Transverse vibrations of an elastically mounted cylinder exposed to an oscillating flow. *J. Offshore Mech. Arctic Eng.* 110 (4), 387–394.
- Trim, A.D., Braaten, H., Lie, H., Tognarelli, M.A., 2005. Experimental investigation of vortex-induced vibration of long marine risers. *J. Fluid Struct.* 21 (3), 335–361.
- Vandiver, J.K., 1985. Drag coefficients of long flexible cylinders. In: Proceeding of the 15th Annual Offshore Technology Conference Houston,TX, No.4490.
- Vandiver, J.K., Swithenbank, S.B., Jaiswal, V., Jhingran, V., 2006. Fatigue damage from high mode number vortex-induced vibration. *Int. Conf. Offshore Mech. Arctic Eng.* 803–811.
- Wang, J., Fu, S., Baarholm, R., Jie, W., Larsen, C.M., 2015. Out-of-plane vortex-induced vibration of a steel catenary riser caused by vessel motions. *Ocean Eng.* 109, 389–400.
- Wang, J., Fu, S., Baarholm, R., Wu, J., Larsen, C.M., 2014. Fatigue damage of a steel catenary riser from vortex-induced vibration caused by vessel motions. *Mar. Struct.* 39 (39), 131–156.
- Wang, J., Fu, S., Wang, J., Li, H., Ong, M.C., 2017. Experimental investigation on vortex-induced vibration of a free-hanging riser under vessel motion and uniform current. *J. Offshore Mech. Arctic Eng.* 139 (4), 041703-041718.
- Williams, J.E.F., Zhao, B.C., 1989. The active control of vortex shedding. *J. Fluid Struct.* 3 (2), 115–122.
- Williamson, C.H.K., 2006. Sinusoidal flow relative to circular cylinders. *J. Fluid Mech.* 155, 141–174.